JPL PUBLICATION 86-38

The TIMS Data User's Workshop June 18 and 19, 1985

National Space Technology Laboratories Mississippi

Anne B. Kahle
Elsa Abbott
Editors

November 1, 1986

National Aeronautics and
Space Administration

Jet Propulsion Laboratory
California Institute of Technology
Pasadena, California

The TIMS Data User's Workshop

Overleaf: TIMS image covering the Saline Valley in eastern central California shows the yellow and green Saline Lake bed in the lower middle. The dark triangular-shaped area is standing water or very wet soil. The Inyo Mountains, composed of granitic batholithic rocks and Paleozoic age sedimentary rocks, form the left edge of the picture. Visible at the upper right are blue-green basalt outcrops and bright-red quartzite and sandstone outcrops and outwash from them. The image has been processed with a decorrelation stretch with channels 1, 3, and 5 displayed as blue, green, and red, respectively.

ORIGINAL PAGE
COLOR PHOTOGRAPH

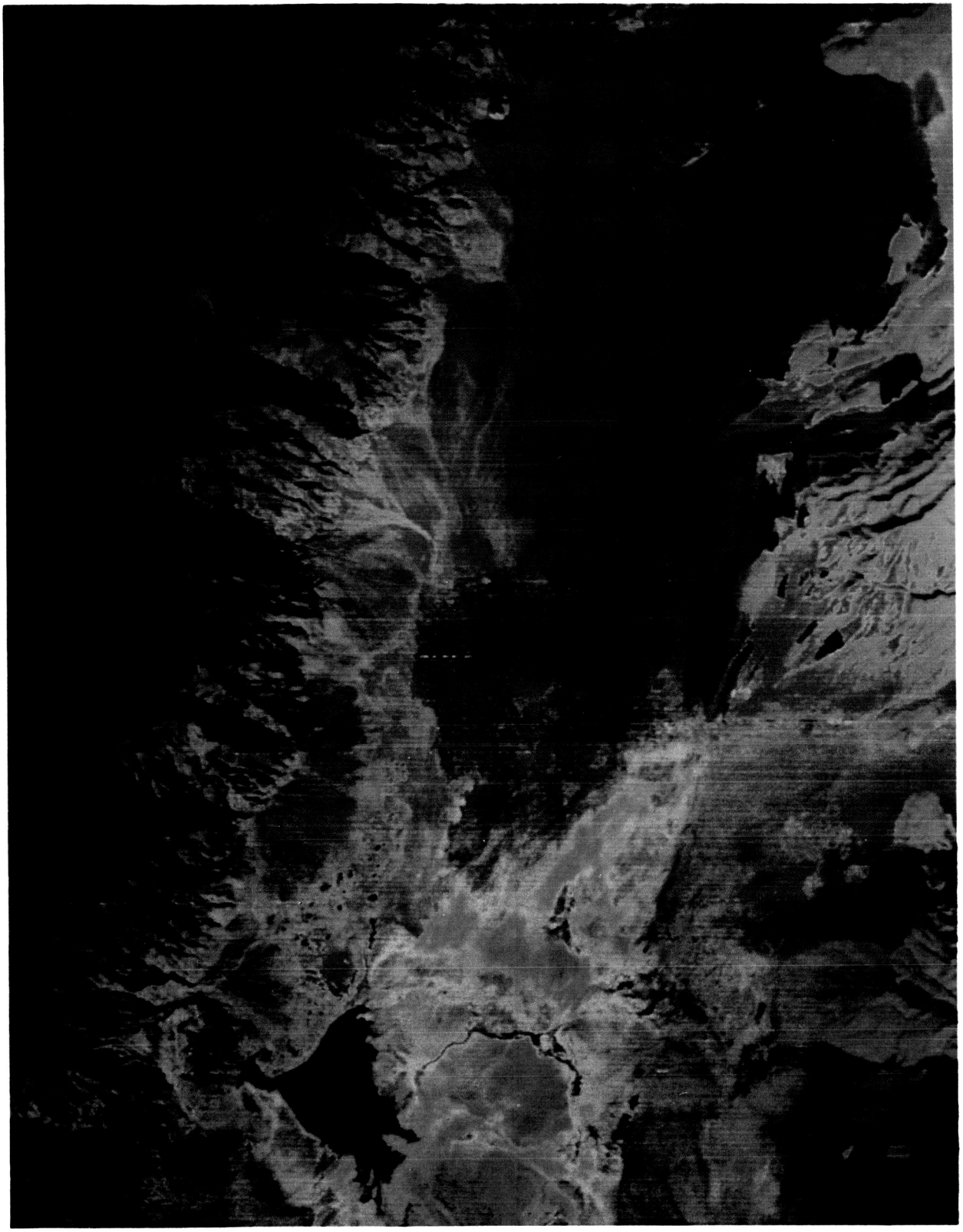

JPL PUBLICATION 86-38

The TIMS Data User's Workshop June 18 and 19, 1985

National Space Technology Laboratories Mississippi

Anne B. Kahle
Elsa Abbott
Editors

November 1, 1986

National Aeronautics and
Space Administration

Jet Propulsion Laboratory
California Institute of Technology
Pasadena, California

This publication was prepared by the Jet Propulsion Laboratory, California Institute of Technology, under a contract with the National Aeronautics and Space Administration.

TABLE OF CONTENTS

ABSTRACT

A workshop was held in June 1985, to bring together users of data from NASA's airborne Thermal Infrared Multispectral Scanner (TIMS). The workshop, organized by the Jet Propulsion Laboratory and held at NASA/NSTL in Mississippi, was successful both for the exchange of ideas between investigators, and to identify issues of concern to the TIMS program. The first half of the workshop was devoted to presentations by the investigators which demonstrated the impressive and unique capability of TIMS. During the second half, the participants formed into working groups to discuss (1) geology, (2) land use, archeology, (3) data processing and noise removal, and (4) future directions of research. These discussions were followed by a summary session, with a presentation from each of the working groups and general discussion of the issues.

One of the major problems identified was that of getting more investigators involved in the program. Suggestions to remedy this included 1) better publicity for the program within the scientific community and 2) better support of the TIMS program by NASA including a structured announcement like an AO or AN to commit NASA funding, and inclusion of the TIMS within the regular structure of the NASA aircraft program, allowing investigators to propose for data flights.

Research issues which need more support include 1) spectroscopic characterization of surface materials including rocks, soils, vegetation, surface coatings, and alteration and weathering products, and creation of a data library 2) surface physical modeling to understand effects of surface emissivity, porosity, grain size, roughness, and mixing laws 3) studies of parameters for future systems such as spatial and spectral resolution, allowable noise, and utility of the 3 - 5 μm window and 4) atmospheric corrections using TIMS data and/or ancillary data. The need for a field instrument was emphasized.

With regard to the future of the TIMS program it was recommended that more use be made of the option of operating TIMS on the C-130 to provide increased range, higher resolution and simultaneous TIMS, AIS and NS001 data, along with generally making the data more available to investigators. At the satellite scale it was emphasized that there is a great potential for TIMS-type data on a worldwide basis and support for it needs to begin now for space shuttle or space platform.

INTRODUCTION

A workshop was held in June 1985, to bring together all the users of data from NASA's airborne Thermal Infrared Multispectral Scanner (TIMS). The workshop was organized by the Jet Propulsion Laboratory, and held at NASA/NSTL in Mississippi.

The purpose of the meeting was (1) to allow users to compare results, data processing algorithms, and problems encountered, (2) to update the users on the latest instrument changes and idiosyncrasies, including distribution of the TIMS investigators guide (Palluconi and Meeks, 1985), (3) to inform the users of the wide range of problems that are currently being tackled by other TIMS investigators, (4) to explore ways to expand the user community, (5) to discuss current areas where more basic research is required, and (6) to discuss future directions of NASA's thermal infrared remote sensing program.

The first half of the workshop was devoted to presentations by the investigators. During the second half, the participants first formed into working groups to discuss (1) geology, (2) land use, archeology, (3) data processing and noise removal, and (4) future directions of research. These discussions were followed by a summary session, with a presentation from each of the working groups and general discussion of the issues.

The participants agreed that the workshop was very successful in meeting its objectives. Short written versions of the investigator presentations are included in this report, followed by an accounting of the topics covered in the discussion session, and finally a summary of the major conclusions reached by the participants concerning the current status and future directions of the program is presented. The agenda and list of participants are in the appendices.

BACKGROUND OF THE TIMS PROGRAM

ANNE B. KAHLE

Jet Propulsion Laboratory
California Institute of Technology
Pasadena, CA 91109

The thermal infrared region of the electromagnetic spectrum available for remote sensing extends from approximately 3 to 25μm. The source of energy is thermal radiation from surface materials at ambient terrestrial temperatures. The spectral range of the usable region is limited by both the amount of energy available and by transmission of this energy through the atmosphere. At terrestrial temperatures, the maximum black body radiation will be somewhere around 10 to 11μm, dropping off sharply to shorter wavelengths and less sharply to longer wavelengths. The best atmospheric window lies between about 8 and 14 μm with poorer windows between 3 and 5μm and between 17 and 25μm. The region between 3 and 5μm is further complicated by overlap with the reflected solar radiation which is dropping rapidly in intensity but still has some contribution in this region. Thus, the 8 to 14μm region is by far the easiest spectral region to use and has received most of the effort to date. Fortuitously, this is also a spectral region containing diagnostic spectral information on many minerals, including the silicates which made up the great majority of continental surface rocks.

The possibility of exploiting the thermal infrared spectral features for remote sensing of rock type from aircraft or satellite has been suggested by many authors (Vickers and Lyon, 1967; Vincent and Thomson, 1972a; Vincent, 1973; Vincent, 1975; Watson, 1975). Vincent and others (1972) and Vincent and Thomson (1972b) flew a scanner having a bandpass between 8.2 and 10.9μm and another bandpass between 9.4 and 12.1μm over a sand quarry near Mill Creek, Oklahoma and over Pisgah Crater, California. They produced ratio images on which they could distinguish between the quartz sand or sandstone and the non-silicate surface material at Mill Creek, and at the Pisgah Crater area, were able to distinguish dacite from basalt and rhyolitic tuff from the surrounding alluvium.

Kahle and Rowan obtained six channels of thermal data in the 8 to 12μm region over Tintic Utah in 1975, using the Bendix 24-channel scanner. Their results were highly successful (Kahle and Rowan, 1980), demonstrating the ability not only to distinguish silicates from non-silicates, but also to make much more difficult separations between silicates, such as monzonite vs. quartz monzonite and latite vs. quartz latite. Unfortunately, due to continuing instrument problems, the scanner was dismantled shortly thereafter.

Based on the great promise shown by the Tintic data, Kahle and Goetz successfully proposed to the NASA geology program in 1981 that the the Thermal Infrared Multispectral Scanner (TIMS) be built. Daedulus

constructed TIMS to meet the Kahle and Goetz functional requirements. Upon completion the instrument was sent to NSTL to be flown on the Learjet, with Kahle designated as the instrument scientist. The personnel at NSTL have done an excellent job of maintaining and upgrading the instrument to remove early noise sources, and in acquiring data for users.

First data flights from TIMS were flown in the summer of 1982, and reported in Science in 1983 by Kahle and Goetz (1983). Subsequently data have been acquired for a number of investigators, some under NASA financed projects and others as reimbursable flights. In 1984 the TIMS was installed on a temporary basis on the NASA/Ames C-130. On this platform it is possible to acquire data simultaneously with the TIMS, the NS001 Thematic Mapper simulator (in the visible and near infrared), and the Airborne Imaging Spectrometer (AIS) - a high spectral resolution visible and near infrared imager. In 1985 such multiple data sets were acquired in Hawaii, Australia, and at a few sites in California, and more will be acquired in Europe in 1986. In between these flights, further TIMS data sets for several U.S. investigators have been acquired from the NSTL Lear jet.

While some papers reporting on TIMS data have found their way into the literature, and a session of the Third ERIM Thematic Conference at Colorado Springs in 1984 was devoted to TIMS, this workshop is the first opportunity for a good fraction of those investigators with TIMS data to meet together to compare results, problems, and ideas for the future.

The research described in this paper was carried out by the Jet Propulsion Laboratory, California Institute of Technology, under contract with the National Aeronautics and Space Administration.

REFERENCES

Kahle, A.B. and L.C. Rowan, Evaluation of multispectral middle infrared aircraft images for lithologic mapping in the East Tintic Mountains, Utah, Geology, 8, 234-239, 1980.

Kahle, Anne B. and Alexander F.H. Goetz, Mineralogic information from a new airborne thermal infrared multispectral scanner, Science, 222, 24-27, 1983.

Vickers, R.S. and R.J.P. Lyon, 1967, Infrared sensing from spacecraft: A geological interpretation, pp. 585-607, in: Thermophysics of Spacecraft and Planetary Bodies, Radiation Properties of Solids and the Electromagnetic Radiation Environment in Space, G.B. Heller, Ed. Academic Press, Inc. New York, 1967.

Vincent, R.K., A thermal infrared imaging method for mapping compositional variations among silicate rock types, Dissertation, Univ. of Michigan, 1973.

Vincent, R.K., The potential role of thermal infrared multispectral scanners in geologic remote sensing, Proc. IEEE, 63, 137-147, 1975.

Vincent, R.K. and F. Thomson, Spectral Compositional Imaging of Silicate Rocks, J. Geophys. Res., 77, 2465-2472, 1972a.

Vincent, R.K. and F.J. Thomson, Rock-type discrimination from ratioed infrared scanner images of Pisgah Crater, California, Science, 175, 986-988, 1972b.

Vincent, R.K., F. Thomson, and K. Watson, Recognition of exposed quartz sand and sandstone by two-channel infrared imagery, J. Geophys. Res., 77, 2473-2477, 1972.

Watson, K., Geologic applications of thermal infrared images, Proc. IEEE, 63, 128-137, 1975.

THE TIMS INSTRUMENT

CHUCK STANICH
DAEDALUS ENTERPRISES, INC.
P.O. BOX 1869
ANN ARBOR, MICHIGAN 48106

I expect that most of the audience is composed of TIMS data users and many of you may not be familiar with the instrument itself. I plan to introduce Daedalus Enterprises, Inc., give background/history on the design and development of TIMS and to cover some of the detailed design considerations. I will provide you with some insights into the design decisions that have taken place and discuss some of the limitations of the system. When I have completed my talk, I would hope that you will be more comfortable with the terminology, concepts, and use of the TIMS airborne line scanner. Possibly some of the information that I will present could find some use in the application of the system.

For those of you not familiar with Daedalus, we were founded in 1968 and are now a publicly-held corporation chartered to pursue all aspects of remote sensing of the environment. We are internationally recognized as the major manufacturer of commercial, airborne optical/mechanical scanner systems. Our systems have been comprised of passive and active systems covering the ultraviolet to the infrared wavelengths and usually are instruments covering one to twelve separate spectral channels. We have designed and delivered systems for four NASA centers: NSTL, MSFC, JSC, and ARC.

The TIMS (Thermal Infrared Multispectral Scanner) system components consist of a scan head/spectrometer and associated electronics.

It was designed as a geologic instrument. In silicate rocks, there is a broad minimum in emissivity between 8 and 11 μm and the depth and position of the band is related to the crystal structure of the constituent minerals. Early attempts to use multispectral image data in this region met with only limited success. In the early seventies, a 24-channel scanner was built for NASA and some promising results were obtained in the thermal infrared region over the East Tintic Mountains in Utah. This scanner reportedly proved to be unreliable and was subsequently dismantled.

After beginning discussions in 1979 with Alex Goetz at JPL, Daedalus was awarded a design study contract for the spectrometer portion of the system in November of 1980. The design consideration given the highest priority was system radiometric sensitivity because the contrast in spectral emittance among rocks is usually less than 15%. After the completion of this design, a contract was received from NASA/NSTL to proceed with the fabrication of the complete system. Before the system was completed, the funds allocated by NASA for the project were depleted. Daedalus then completed the system using its own funds and it was test flown and delivered in March of 1982.

The system has been maintained and modified by NASA since then and possibly some of the information that I will present may not apply to the current TIMS configuration.

A NASA/NSTL Learjet has been specially modified to accommodate the TIMS system. The system normally is flown using this aircraft although it has also been operated in the NASA/ARC C-130 aircraft. The scan head and spectrometer are mounted in the unpressurized tail cone of this aircraft and operate through a hole cut through the skin. The fact that the system would be exposed to the environment outside the skin of the aircraft was an important consideration in the design process.

We feel that the system is quite compact considering the achieved sensitivity. The scan head/spectrometer is slightly over three feet long, 30 inches high and weighs over 220 pounds. The temperature over which the scan head/spectrometer can operate is very large. The number of spectral channels covered is six ranging from 8.2 μm to 12.2 μm. The original specification of the system required a sensitivity of less than .3K in each of the bands. When the system was delivered to NSTL, all bands had a sensitivity of less than .2K with the exception of band 6.

The entrance aperture to the primary optics is 7.5 inches in diameter resulting in an effective collecting area of 36 sq. inches. The system has a variable scan rate which is switch selectable by the operator. The scan rates can be varied from 7.3 to 25 scans/second by adjusting the rotation rate of the scanning mirror to accommodate the different speeds and altitudes of the aircraft.

The digitized field of view contains 638 pixels and covers 76.56 degrees. This digitized field of view is adjusted according to the roll attitude of the aircraft in order to stabilize the image. The unvignetted field of view relates to how large the total optical view can be before an obstruction to the optical path is encountered. Comparing the digitized field of view with the unvignetted field of view would indicate that the system can accommodate approximately 1.5 degrees of roll before a pixel from the edge of the scene will be lost. However, a total of +- 15 degrees of roll can be handled before stabilization of the scene pixels is lost.

The system digitizes each pixel to 8 bits, and the detector analog signals are sampled every 2.08 milliradians. The instantaneous optical field of view is 2.5 milliradians as determined by a field stop aperture which is common to all of the spectral channels. This common aperture ensures that all of the channels are in spatial registration. The output data rate varies from 44 to 150 kbits/sec and each scan line of each channel contains 750 words. The output data is recorded on a wide band instrumentation tape at a density of 10,000 bits per inch per channel.

The scan head contains the primary collecting optics of the system and the two thermal reference sources, determines the instantaneous field of view, receives the motor drive signal for the scanning mirror, and provides an optical and mechanical interface to the spectrometer. The spectrometer collimates the optical energy received from the primary, disperses it using a diffraction grating and focuses the energy onto a series of liquid nitrogen cooled detectors.

The electrical output of the detectors is coupled to the digitizer where the amplitude is adjusted, bandwidth limited, sampled, digitized, and monitored. The digitizer also receives various housekeeping information about the

system and aircraft and combines this with the video data from the detectors and conditions it for use by the tape recorder.

The control console is used by the operator to monitor system activities and to control the system functions. The scan speed selection by the operator is distributed to the various units from the control console. The console also accepts the signals from the scan motor encoder and the gyro to perform the roll stabilization. Controls for the two thermal reference sources are contained in the control console.

The assemblies of the scan head are the dc motor, the mirror and the encoder. All timing related activities are synchronized to the encoder including the digitization and tape recorder speed. A gyro is used to determine the roll attitude of the aircraft. The thermal reference sources are mounted on each side of the scan head and consist of large copper plates which are painted black with a paint that has a high emissivity throughout the spectral region. One reference can be set to either above or below the scan head ambient temperature while the other one can only be set to a temperature above the scan head ambient. Each reference is actively controlled and the source temperature is independently measured and inserted into the housekeeping data associated with each channel.

The spectrometer contains the dispersing optics and the array of photoconductive cooled detectors. A set of six electrical preamplifiers are matched to each element of the array and are mounted onto the side of the spectrometer. The spectrometer is sealed and purged with a supply of dry nitrogen gas during each flight.

The TIMS optical system consists of a 19 cm diameter Newtonian reflector telescope mounted behind an object-plane 45^{o} flat scanning mirror and followed by a Czerny-Turner spectrometer.

The primary optical system uses a f1.9 parabolic primary mirror with a field determining aperture located in its focal plane. An off-axis parabolic mirror is used to collimate the energy emerging from the aperture which is then dispersed by the diffraction grating and re-imaged on the detector array by a fast f0.6 germanium lens. All of the primary optical elements, the field stop, the off-axis collimator, and the detector dewar are mounted on sliding blocks controlled by Invar^{R} metering rods to provide the active thermal compensation for scan head ambient temperature changes. The three element germanium imaging lens is also internally thermally compensated for changes in ambient temperature.

The TIMS Investigator's Guide*

Frank D. Palluconi
Jet Propulsion Laboratory
California Institute of Technology**
Pasadena, California 91109

The purpose of this guide is to provide in one location, enough information about the Thermal Infrared Multispectral Scanner (TIMS) that potential investigators can decide whether or not it would provide measurements useful in their research program and to provide a new user of TIMS data sufficient information to begin analysis.

TIMS is a NASA aircraft scanner providing six-channel spectral capability in the thermal infrared region of the electromagnetic spectrum. Operating in the thermal infrared atmospheric window region (8-12 μm) with a sensitivity of approximately 0.1°C TIMS may be used whenever an accurate measurement of spectral radiance or brightness temperature is needed.

The channel locations (full width at half maximum) measured in June of 1984 are: channel (Ch) 1 8.2-8.6, Ch 2 8.6-9.0, Ch 3 9.0-9.4, Ch 4 9.6-10.2, Ch 5 10.3-11.1, Ch 6 11.3-11.7 in micrometers. The peak of ozone absorption is contained within the bandpass of channel 4. The cross-track digitized field-of-view is 76.56°, covered in 638 eight-bit samples (for each channel). Each sample is thus spaced 2.094 mrad from the next. The instantaneous field-of-view is 2.5 mrad. Any one of four scan rates (7.3, 8.7, 12, 25 scans/second) may be selected to provide the desired ground resolution in conjunction with the aircraft speed and altitude. Two temperature controlled reference plates are contained within the instrument. One is sampled at the beginning of every scan and the other is sampled at the end of every scan. This permits scan by scan calibration of the data leading to highly accurate estimates of spectral brightness temperature.

Investigators interested in using TIMS may propose such use through the Earth Science and Applications Division of NASA's Office of Space Science and Applications. The "Guide" provides forms for making specific flight requests, a description of the raw and reduced record formats and a procedure for converting the recorded data to spectral radiance or spectral brightness temperature.

* Infrared Multispectral Scanner (TIMS): An Investigator's Guide to TIMS Data, Palluconi, F. D. and Meeks, G. R., JPL Publication 85-32 (JPL, 4800 Oak Grove Drive, Pasadena, CA, 91109) 32 pp.

** The research described in this abstract was carried out by the Jet Propulsion Laboratory, California Institute of Technology, under contract with the National Aeronautics and Space Administration.

Estimation of Absolute Water Surface Temperature Based on Atmospherically Corrected Thermal Infrared Multispectral Scanner Digital Data

James E. Anderson
Research Forester

National Aeronautics and Space Administration
National Space Technology Laboratories
Earth Resources Laboratory
NSTL, MS 39529

Airborne remote sensing systems, as well as those on board earth orbiting satellites, sample electromagnetic energy in discrete wavelength regions and convert the total energy sampled into data suitable for processing by digital computers. In general, however, the total amount of energy reaching a sensor system located at some distance from the target is composed not only of target related energy, but, in addition, contains a contribution originating from the atmosphere itself (through which the target related energy must pass). Thus, if a researcher is particularly interested in dealing with target-related energy exclusively, some method must be devised for removing or at least minimizing the effect of the atmosphere.

For the purposes of this project, LOWTRAN-6, an atmospheric path radiance model developed by the Air Force Geophysics Laboratory, was used. This model was "designed to estimate atmoshperic transmittance and radiance for a given atmospheric path at moderate spectral resolution" (Kneizys, et al., 1983) over an operational wavelength region from 0.25 to 28.5μm.

In order to compute the TIMS digital values which would have been recorded in the absence of the atmosphere, the parameters derived from LOWTRAN-6 are used in a correction equation of the form:

$$y' = \left[\frac{y - m(\cos\alpha)^{p'} EA - b}{\bar{\tau}(\cos\alpha)^{p}} \right] + b$$

where y is the corrected digital value
m is the slope of the System Transfer Equation
b is the intercept of the System Transfer Equation
α is Angle of Look from Nadir
EA is additive atmospheric path radiance
E is average atmospheric transmissivity
p,p' are exponents defining behavior of $\bar{\tau}$ and EA, respectively.

TIMS data used to test this technique were collected at 1:00 a.m. local time on November 21, 1983, over a recirculating cooling pond for a power plant in southeastern Mississippi. Twenty-two floating thermometers provided ground truth, and were read within + 10 minutes of TIMS data acquisition. Readings taken earlier in the day indicated that thermometer measurements were stable over a much longer (1 hour) time frame, so that errors from the time span encompassing ground truth data acquisition were minimal.

The TIMS data were analyzed before and after atmospheric corrections were applied using a band ratioing model to compute the absolute surface temperature of various points on the power plant cooling pond. The results summarized in Table 1, clearly demonstrate the desirability of applying atmospheric corrections, and while tested using water as a target, the technique developed is also applicable to vegetated targets.

	Before Atmospheric Correction	After Atmospheric Correction
Multiple R^2	0.942	0.985
Peak-to-peak residuals	$\pm 1.0^{o}C$	$\pm 0.4^{o}C$
Sample size (thermometers)	22	22

Table 1. Results of a Linear Regression of Estimated (Predicted) Water Surface Temperatures Versus Actual (Observed) Temperature Determined Through the Use of Floating Thermometers. TIMS Channels 2 and 5 Used for Analysis.

Reference

Kneizys, F.X., E.T. Shettle, W.O. Gallery, J.H. Chetwynd, Jr., L.W. Abru, J.E.A. Selby, S.A. Clough, and R.W. Fenn, 1983, Atmospheric Transmittance/Radiance: Computer Code LOWTRAN 6, Optical Physics Division, Air Force Geophysics Laboratory, Hanscom Air Force Base, Massachusetts, 01731, Report No. AFGL-TR-83-0187, 200 pp.

Atmospheric Correction of TIMS Data

Doug Rickman

National Space Technology Laboratories
Earth Resources Laboratory
NSTL, Mississippi 39529

The TIMS is a unique sensor for two reasons, it is multispectral in the thermal-IR and it has on board, active calibration sources. The existence of the calibration permits the recorded DN's to be converted unambiguously to absolute energy units. However, to relate the data to energy originating from a target on the ground it is necessary to remove the atmosphere's contribution to the signal, specifically its transmittance and emittance. These can be obtained fairly easily by use of the atmospheric model provided by LOWTRAN-6 and the data from the U.S. Weather Service's network of bi-daily radiosondes. Using these data with the TIMS responsivity curves an equation can be obtained which permits the unambiguous correction of the TIMS data for the atmosphere.

$$DV_T = \int(SR_\lambda)d\lambda \cdot \left[\frac{DV_r - m\cdot\int(SR_\lambda \cdot E_{RA_\lambda})d\lambda - b}{\int(SR_\lambda \cdot \tau_{A_\lambda})d\lambda}\right] + b$$

DV_r - recorded digital value

DV_T - corrected digital value, the "true or proper" digital value for the target

E_{RA_λ} - energy radiated by the atmosphere by wavelength

m - slope of system transfer equation (gain)

b - offset of system transfer equation

τ_{A_λ} - transmissivity of the atmosphere by wavelength

SR_λ - sensor responsibility by wavelength

ENHANCEMENT OF TIMS IMAGES FOR PHOTOINTERPRETATION

A.R. Gillespie

Geology Group
Jet Propulsion Laboratory
California Institute of Technology
Pasadena, California 91109

ABSTRACT

TIMS images consist of six channels of data acquired in bands between 8 and 12 μm; thus they contain information about both temperature and emittance. Scene temperatures are controlled by the reflectivity of the surface, but also by its geometry with respect to the sun, time of day, and other factors unrelated to composition. Emittance is dependent upon composition alone. Thus the photointerpreter may wish to enhance emittance information selectively. Because thermal emittances in real scenes vary but little, image data tend to be highly correlated among channels. Special image processing is required to make this information available for the photointerpreter. Processing includes noise removal, construction of model emittance images, and construction of false-color pictures enhanced by decorrelation techniques.

INTRODUCTION

Thermal infrared radiance measurements historically have been used to estimate temperatures of surfaces. Thermal infrared images have generally been used the same way. Thermal radiance is related to the temperature of a surface through Planck's Law and a proportionality factor known as the thermal emissivity or emittance. The temperature is a function of a number of factors. Among these are: reflectivity in visible and near-infrared wavelengths, thermal inertia of the material composing the surface, the geometry of the surface with respect to the sun, the time of day, and various characteristics of the atmosphere. Some of these factors - the reflectivity and thermal inertia - are intrinsic properties of the composition of the exposed material. Other factors are properties of the surface itself. Still others have nothing to do with the surface, but depend on the weather, time of day, and so forth. Thus radiance images convey much information, but not necessarily in a simple way.

Thermal emittance of the earth's surface, on the other hand, is controlled largely by the composition of the surface material, by the texture of the surface, and by the local topography, independent of lighting conditions, weather, or time of day. Furthermore, emittance varies with wavelength in a way that is

distinctive for many silicate and other rock-forming minerals [Lyon, 1965]. Thus emittance spectra are a useful aid in lithologic mapping and other geologic studies.

TIMS images are multispectral; they consist of six channels of radiance data acquired in bands between 8 and 12 μm [Palluconi and Meeks, 1985]. Thus they contain information about both the temperature of a surface, and also its emittance spectrum.

The photointerpreter has at his disposal a wealth of information in TIMS images. If he is interested in surface composition, he may chose to enhance emittance information selectively. Because thermal emittances in real scenes vary but little, image data tend to be highly correlated among channels. Special image processing is required to make this information available for the photointerpreter. Processing includes noise removal, calculation of model emittance images, and construction of false-color pictures enhanced by decorrelation techniques.

ENHANCEMENTS

Noise Removal

TIMS data contain noise from a number of sources. In addition to random detector noise, which has an NEΔT of ~0.2° at 300 K [Palluconi and Meeks, 1985], there is found both low- and high-frequency striping, microphonic interference and a signal-dependent bit error in one preamplifier (Ch. 6). Some of these components may be removed by the appropriate image-processing technique, but each requires a different approach.

Random Noise... Random detector noise is intrinsically part of the image data. The dynamic range is chosen such that the noise level is generally ±1 DN. Pixels having DN that are radically different than neighboring values can be recognized and removed with a variety of techniques, most notably median filtering. Approaches such as this will also remove "deviant" or unusual signal, however. In general, the amplitude of random detector noise in TIMS is too low to warrant efforts to suppress it.

Bit Errors... Unlike the low-amplitude random noise, bit errors are obvious defects in the TIMS data. They appear to occur when there are strong and rapid changes in the scene radiance; thus the bit errors will often be encountered on one side of a sharp high-contrast feature in a scene. They are generally removed by bilinear interpolation, in algorithms that compare local to neighboring DN values. Local values that exceed the mean DN of the neighboring pixels by more than a settable threshold are replaced by the mean DN itself. Median filters also are effective at suppressing this type of noise.

Bit errors seem to occur infrequently, but their tendency to be grouped along interesting image features (edges) is disruptive to

photointerpretation. Therefore their removal is usually helpful.

Low-Frequency Striping... TIMS data frequently contain a low-amplitude, low-frequency striping or banding that is attributed to changes in detector sensitivity. Although the striping is so subtle (<10% of the encoded radiance) that it may be difficult to see in images made from the radiance data, it tends to be poorly correlated among channels. Therefore this striping is "colored;" it masquerades as scene emittance changes. In fact, the amplitude of this source of noise in emittances may be so high that it is the greatest source of variance in the emittance images. False-color images made from calculated emittance values may be dominated by the low-frequency striping. In these pictures the low-frequency striping looks like varicolored horizontal bands or bars about 200 image lines high. Because emittance is often the parameter of greatest interest in TIMS data, this striping is a serious problem. For photointerpretation, striping removal is desirable. For calculating meaningful emittance data, removal is necessary.

Fortunately, TIMS scans a hot and a cold blackbody of measured kinetic temperatures once per image line. Since the detector response to the thermal photon flux is linear [Palluconi and Meeks, 1985], this information is adequate to calibrate the detectors line by line. The procedure is simple: The photon flux from the reference blackbodies for each TIMS channel is calulated using the measured temperatures, the spectral sensitivity of the detectors and filters, and Planck's Law. From this information the linear equation relating the DN values reported for the blackbodies to the calculated fluxes is found. This will vary from scan line to scan line. Then the photon fluxes for the image pixels are found, using the reported DN values and the linear coefficients found from the calibration data.

Use of the TIMS on-board calibration data as described above is effective in suppressing the low-frequency striping due to detector sensitivity changes. In enhanced pictures the banding will no longer be visible. But some extra precautions are necessary in processing to avoid *introducing* additional high-frequency striping during banding suppression. The problem arises because, like the image data, the calibration data are contaminated by microphonic noise and occasional dropped bits. Obviously, if the data used to calibrate the image are themselves in error, striping removal will be ineffectual or worse. However, because the detector sensitivity changes slowly, any high-frequency fluctuations in the calibration data must be caused by noise. Drop-outs may be removed from the calibration data by median filtering; then high-frequency microphonic noise may be removed by low-pass filtering in either the spatial or frequency domain. These precautions should always be taken.

High-Frequency Striping... A major source of high-frequency striping in TIMS data is microphonic vibration of the detector, which sits on a long stem in its dewar. In one TIMS image of Newfoundland, microphonic noise was oblique to the scan lines and

had wavelengths of 200 samples and 25 lines per cycle (Figure 1). The exact frequencies are variable, even if the image is acquired at the same scan rate. Obviously, the angle of the striping and its frequency in the scan direction vary with the scan speed selected during data acquisition by the technicians operating TIMS.

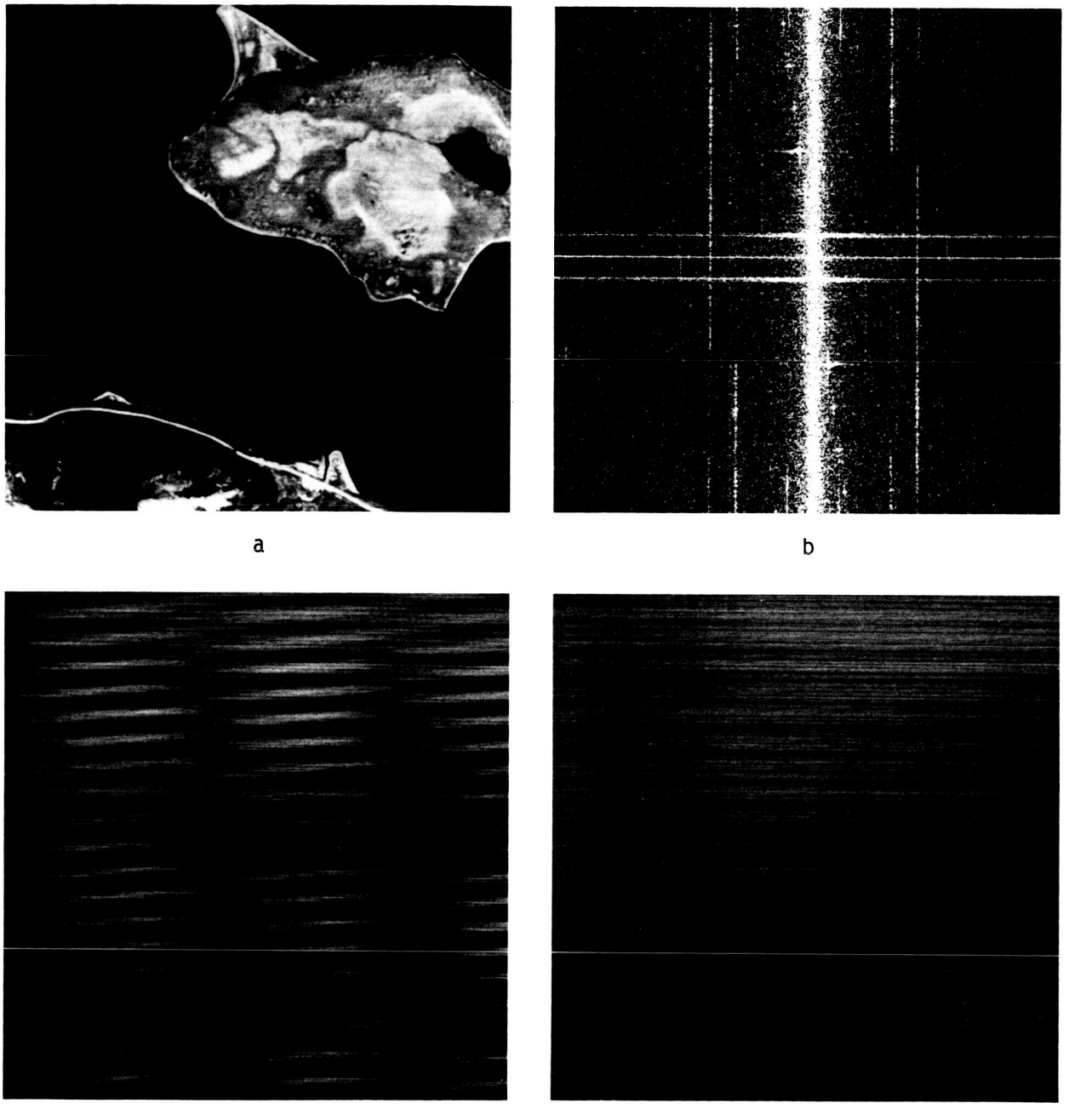

Figure 1. A TIMS image of Newfoundland, showing noise. (a) Radiance image. (b) Two-dimensional Fourier transform of an image subscene. The modulus is displayed as black (zero) to white (high). Frequencies vary from zero (origin, at center) to 0.5 cycles/pixel (edge). Horizontal axis displays frequencies in the scan direction. (c) Microphonic noise removed from the image. (d) residual striping in image after microphonic noise was removed.

Figure 1 shows (a) a TIMS image of Newfoundland, (b) a two-dimensional Fourier transform of the image data, (c) the microphonic noise found in the image, and (d) residual horizontal striping that remained after the microphonic noise was removed. Very little microphonic noise is seen in the radiance image. However, the Fourier transform shows large bands and spikes that correspond to the noise. Additionally, the transform has large amplitudes on the axes. These occur if there are radiance gradients across the image, because of the periodic nature of the transform. Finally, this particular image was geometrically corrected before it was transformed, to compensate for panorama foreshortening. This has the effect in the transform of spreading out noise spikes in the scan (horizontal) direction.

Most of the image data are concentrated in a continuum near the origin of the transform. The obvious noise in Figure 1d has frequencies that plot near the continuum also, a little more than 1 pixel away in the scan direction and ~20 pixels away in the line direction (1st and 3rd quadrants). The microphonic noise is not spectrally pure, and its dominant frequencies are not necessarily simple integer factors lower than the Nyquist frequency. Because of these effects, the dominant noise spike is distributed in a cross, orthogonal to the coordinate system. In this instance, scan-direction smearing by the geometric corrections discussed above appears to have been significant.

The noise images shown in Figures 1c,d were isolated using the techniques described below. The source of the residual striping is uncertain. Some of it may result because of changes in detector sensitivity during the interval between measurement of the internal reference and measurement of the scene. High-frequency striping in TIMS data is variable in amplitude; it is not always a dominant component of the image. However, as with the banding due to changing detector sensitivity, even subtle striping is exaggerated by processing the image to extract emittance data, or in constructing radiance ratio images. Below, ratioed radiance data from a relatively noise-free TIMS image of Death Valley, California, are used to illustrate high-frequency striping removal by filtering in the frequency (Fourier) domain.

Figure 2 shows the TIMS image of Trail Canyon Fan, across Death Valley from Monument Headquarters at Furnace Creek. An enhanced false-color picture of this image is in Kahle and Goetz [1983] or in Gillespie et al. [1984]. Figure 2a is the ratio picture of TIMS channels 5/6, before noise removal. The microphonic noise is nearly diagonal in this picture, with a wavelength of ~50 pixels. Additional, subhorizontal high-frequency striping is evident. Finally, bit errors (dark in Channel 6) appear as bright spots, especially evident on the west sides of the dark regions on the valley floor. The bit errors were identified and removed using the approach discussed above, before transforming the image to the Fourier domain. Figure 4b shows the Fourier transform of the ratio image. The obvious microphonic noise is confined to two horizontal bars near the horizontal axis, as for the Newfoundland image, and for the same reasons.

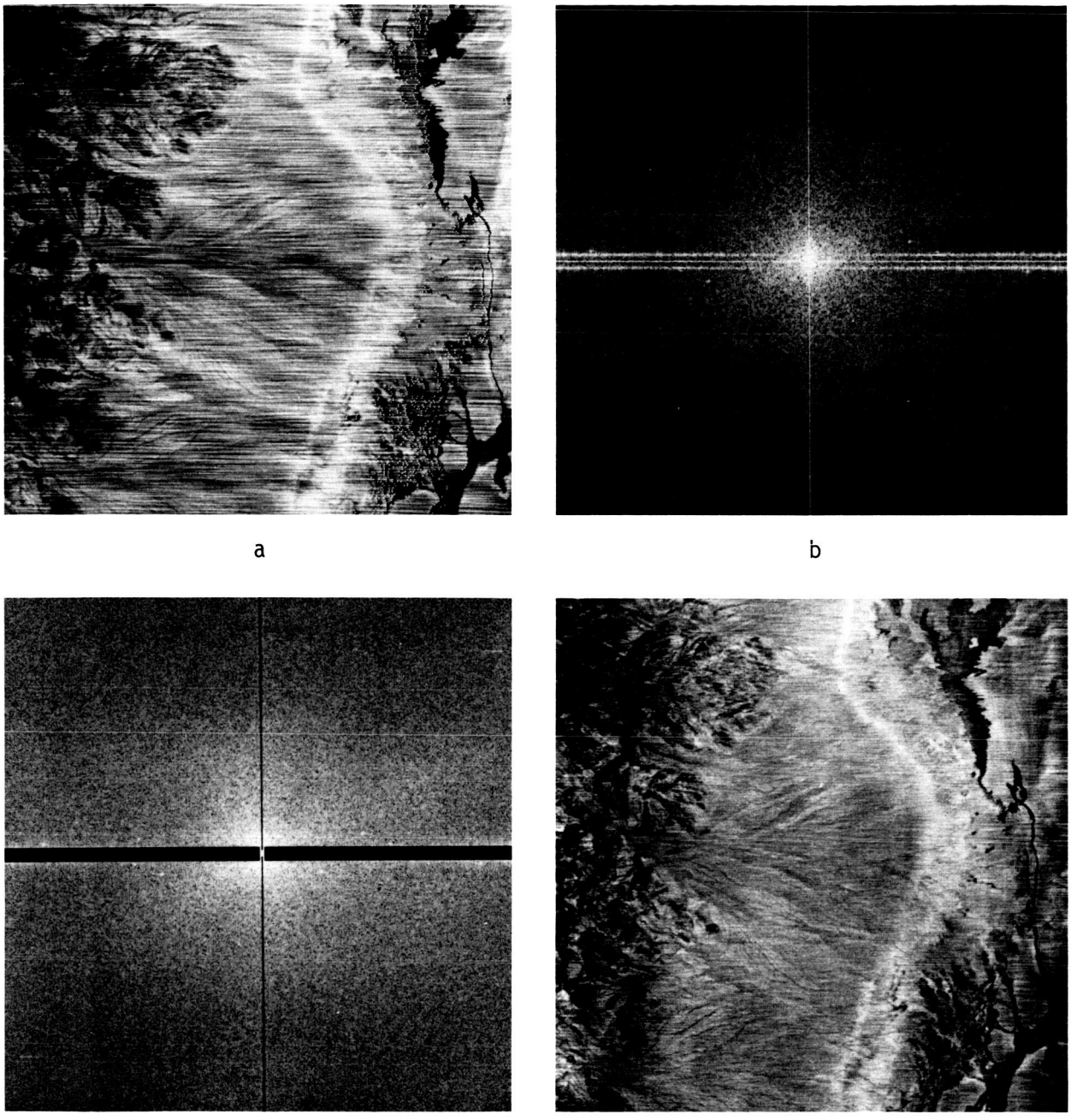

Figure 2. TIMS image of Death Valley, California. (a) Ratio picture, Channels 5/6, showing microphonic noise. (b) Fourier transform. (c) Fourier transform with noise masked out. (d) Ratio image with microphonic noise removed.

Filtering in the Fourier domain is readily accomplished by multiplying the transform by a mask (the filter) that passes or rejects data. It is not necessary that the filter be a binary function, but for this example it was. Figure 1c shows the filtered transform of Figure 1b. The filter multiplied by zero those image components that plot on the vertical axis or near the

horizontal axis (except very near the origin). The filtered image was then reconstructed by performing a Fourier transformation on the filtered transform (inverse transformation). The filtered ratio picture is shown in Figure 1d. Cursory inspection shows that most of the microphonic noise has been suppressed.

Detailed inspection of the filtered image of Figure 1d reveals a number of directional artifacts that appear as an oriented fabric [Gillespie, 1980]. These undesired artifacts are consequences of removing too much power from the image near the zero-frequency axes. The fabric can be suppressed using a more complicated filter that passes data in a narrow horizontal bar within the suppressed bar of Figure 1c. These results are not shown here.

Filtering in the Fourier domain is a conceptually simple approach to removing noise in digital images that has been successfully used on a wide range of projects [e.g., Rindfleisch et al., 1971]. There are drawbacks, however, for the user of small computers. The transform is computationally expensive; the fast Fourier transform (FFT) requires the period of the image chip to be a power of two. The TIMS data are not. There are ways to solve this problem: the image may be "padded" with gray data to widen it; it may be truncated to make it smaller; or the FFT need not be used to perform the transformation.

Another approach is to filter the image in the spatial domain (as acquired), by convolution. In general, two-dimensional convolution is an expensive procedure, but because most of the noise in the TIMS data is subparallel with either the scan or the flight axis only a one-dimensional filter is required. The weights in the filter kernel are found from the 1-D transform of the frequency-domain filter discussed above. These may be calculated analytically, for simple filters [e.g., Castleman, 1979].

The general equation for a 1-D spatial-domain filter kernel that has the same effect as the binary filter discussed above is given by:

$$h(x) = \delta(x) - 2\Delta s \frac{\sin(\pi \Delta s\, x)}{\pi \Delta s\, x} \cos(2\pi s_o x) \qquad (1)$$

where **h** is the filter kernel, **x** is the kernel sample value in the scan or flight direction, as appropriate, and **s** is the frequency in the transform. The filter kernel is centered at **x = 0**. The Kronecker delta function **δ(x)** is an all-pass filter:

$$\left[\begin{array}{l} \delta(x) = 1 : x = 0 \\ \delta(x) = 0 : x \neq 0 \end{array} \right] \qquad (2)$$

Kernel **h(x)** is a high-pass filter. The frequencies that are not passed by **h(x)** are specified by the right-hand terms of equation

1: s_o is the central frequency to be suppressed, and Δs is the range of frequencies centered on s_o to be suppressed. The cosine term is the transform of the impulse pair at s_o in the frequency domain. The sinc function is the transform of a rectangular pulse of width Δs (in the frequency domain).

Now for the discrete transform of an image of **NS** samples, the frequency interval Δs corresponding to a sample interval Δx in the transform is given by:

$$\Delta s = \frac{\Delta x}{NS/2} \quad 0.5 \quad = \quad \frac{\Delta x}{NS} \tag{3}$$

The factor of 0.5 in Equation 3 is the Nyquist frequency. Thus, if we suppress the smallest range of frequencies possible in the discrete transform of a 1024-sample image ($\Delta x = 1$), $\Delta s = 1/1024$ and

$$h(x) = \delta(x) - \frac{\mathrm{sinc}(\pi x/1024)}{512} \cos(2\pi s_o x) \tag{4}$$

Weights for the convolution filter may be found from equation 4, or a similar expression if other filter characteristics are desired.

Convolution filtering has two noteworthy drawbacks: first, the filters will "feel" the edge of data when they are half their width from an edge. This results in a bright or dark artifactual band down the sides of the image (horizontal filter) or along the top and bottom (vertical filter). This artifact can be reduced in severity by reflecting the image about its limits and filtering the reflected data, together with the actual image, but additional computational cost is incurred.

A second problem is that if it is necessary to suppress a narrow band of frequencies (Δs is small, as in equation 4), the number of weights required is large. If too few filter weights are used the filter will not pass the data accurately; it also may "ring," or sense high-contrast features in the image when it is centered some distance away. Ringing caused by a poorly designed filter can be quite annoying to the photointerpreter (Figure 3). It can be reduced by using a frequency-domain filter with softer edges than the binary mask; e.g., weights described by a Gaussian function. In this case, the right-hand terms in Equation 1 must be multiplied by the transform of the new function (in this example, another Gaussian function) instead of the sinc function.

Although this practice was not followed in producing the examples used above, it is important to filter the image before panorama correction. In this way, the noise is not dispersed throughout the spectrum, and the filter can be designed to remove less signal.

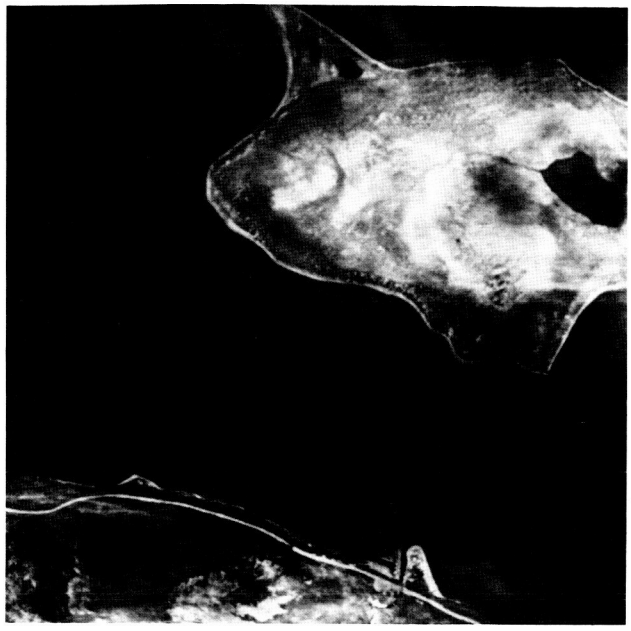

Figure 3. The TIMS image of Newfoundland (Fig. 1a), filtered by convolution with a 1-D filter kernel that induced excessive "ringing" off hard edges.

Analysis: Model Emittance Calculation

Once the noise has been removed from the TIMS data, and the images have been calibrated in units of photon flux, they are ready for analysis. In geological applications, the emittance (ε) information imbedded in the radiance data is of great significance, because it is related to the composition of the imaged surface, especially for silicate rocks. On the other hand, the temperature varies with topography, and throughout the day. It is only indirectly related to the surface composition. Thus it is desirable to separate temperature and emittance information.

Unfortunately, with six channels of data and seven unknowns (six emittance values and the temperature) the problem is underdetermined. We must make an assumption in order to calculate anything at all. The assumption generally made is that the emittance ε_6 channel 6 (with a bandpass centered at ~11 μm) is known. Its value ε' is generally taken to be about 0.93 (emittance ranges from 0 to 1), thought to be typical for a wide range of silicate minerals. However, this assumption is generally not true for mafic and ultramafic silicate rocks, and this must be remembered in interpreting emittance data calculated this way. In general, it is useful to identify emittances ε' calculated from thermal IR scanners as "model emittances," so that the basic assumption is not overlooked.

The temperature T at which the surface is radiating is approximated using Planck's Law, for the photon flux or radiance

R in Channel 6:

$$T_6 = \frac{c_2}{\lambda_6}\left[\ln\left[\frac{\varepsilon_6' c}{R_6 \lambda_6^4} + 1\right]\right]^{-1} \quad (5)$$

where λ_6 is the wavelength for channel 6. Strictly, there is no single value of λ_6, because the bandpass for channel 6 is 11.2-12.2 μm, so in order to calculate R_6 Planck's Law must be integrated over λ. Equation 5 would be accordingly more complicated, but for the purposes of this discussion it is simplified by assuming that the bandpass is quite narrow and there does exist a single value for λ_6.

Parameter $c_2=ch/k$ in equation 5 is a constant, and ε_6' is the emittance assumed for channel 6. The parameter **c** is the speed of light; **h** is Planck's constant; and **k** is Boltzmann's constant. Because the TIMS detectors respond to the photon flux, rather than the energy [Palluconi and Meeks, 1985], the right side of equation 5 has been divided by a factor of hc/λ (the energy for a photon of wavelength λ).

Once T_6 is estimated, model blackbody values of R_i' can be calculated for channels 1-5, according to:

$$R_i'(T_6) = \frac{c}{\lambda_i^4}\frac{1}{\{\exp[c_2/(\lambda_i T_6)] - 1\}} \quad (6)$$

Emittance ε is the proportionality constant between observed radiance and the ideal radiance from a blackbody at the same kinetic temperature. Therefore, we may calculate model emittances ε_i' according to

$$\varepsilon_i' = \varepsilon_6' \frac{R_i}{R_i'} \quad (7)$$

Images made of model emittance data show little topography or temporal heating patterns; they show largely compositional information. Pictures of such emittance data for Death Valley are given in Kahle and Walker [1984].

As mentioned above, the assumption that $\varepsilon_6' = 0.93$ is not valid for mafic rocks; measured values are lower. Thus emittance data for some channels of TIMS data may exceed unity over ultramafic and mafic rocks. What has happened is that the reststrahlen band (Si - O vibration) has shifted to longer wavelengths in mafic minerals. Consequently, for mafic minerals a better assumption would be that $\varepsilon_i = 0.93$ [e.g., Lyon, 1965]. It is computationally simple to find the channel for which the apparent T_i is maximum. If we assume a value for the maximum ε, and not

restrict the channel for which it is found, we can calculate reasonable values of ε' regardless of the type of silicate rock in the scene.

Finally, it may be useful to estimate the wavelength of the reststrahlen band and report that information as an image. Gillespie and Abbott [1984] showed that this parameter is sensitive to silicate mineralogy in a range of TIMS images. They estimated the central wavelength of the reststrahlen band by fitting a Gaussian function to the emittance data. Other reported parameters were the width of the reststrahlen band (standard deviation) and the intensity (difference between minimum and maximum emittance values).

Decorrelation Stretching

Commonly, it is desired to display false-color pictures made from three selected channels of TIMS data. It is easier to interpret these data if some topographic (temperature) data is left in the pictures. Also, if noise removal is incomplete, or for very noisy data, the emittance data will be heavily striped.

Soha and Schwartz [1978] devised a technique to exaggerate the highly correlated emittance information, while retaining some of the temperature information. They called this method the "decorrelation stretch" because it involved calculating statistically independent or orthogonal images in which the covariance was zero. This was done by principal-component analysis.

Early efforts to use principal-component images as red-green-blue (**RGB**) components of false-color pictures were successful in producing brightly colored pictures, but these were hard to interpret in terms of physical processes in the scene. Soha and Schwartz intended to produced a false-color picture in which there was little distortion of hue, but in which color saturation or chroma was exaggerated and the intensity or lightness was suppressed. This they did by equalizing the variance in the principal-component images, and then applying the inverse transformation to recreate the images in the original **RGB** domain. False-color pictures made from "decorrelation-stretched" images were colorful, but could easily be related to the original images or to spectral data describing the scene. An example of a "decorrelated" false-color picture may be found in Kahle and Rowan [1980]. A thorough discussion of the method may be found in Gillespie et al. [1986].

SUMMARY

TIMS data can be used both for photointerpretation and scene analysis, but careful processing is in general necessary before they may be used. This processing involves image calibration to suppress effects due to detector sensitivity changes, and filtering to remove microphonic and other high-frequency striping

noise. Additionally, it may be necessary to identify bit errors in the image and remove them by interpolation. Once the image is free of artifacts, additional processing is necessary to separate emittance and temperature information. This is desirable because emittance information describes the composition of the imaged scene, especially if it contains silicate minerals. Wavelengths of reststrahlen bands may be estimated from emittance data by curve-fitting techniques. This information is related to rock type. Alternatively, images may be prepared for photointerpretation by "decorrelating" them before contrast-stretching and construction of false-color pictures.

ACKNOWLEDGEMENTS

NSTL personnel, particularly G. Meeks, have been unstinting in their support, operation, and improvement of TIMS. The research described in this paper was carried out at the Jet Propulsion Laboratory of the California Institute of Technology and sponsored by the Land Processes Branch of the National Aeronautics and Space Administration.

REFERENCES CITED

Castleman, K., 1979, Digital Image Processing, Prentice Hall, New York, pp 139-225.

Gillespie, A.R., 1980, Digital techniques of image enhancement, in Siegal, B.S., and A.R. Gillespie, *eds.*, Remote Sensing in Geology, Wiley, New York, pp 216-219.

Gillespie, A.R. and E.A. Abbott, 1984, Mapping Compositional Differences in Silicate Rocks with Six-Channel Thermal Images, Proc. 9th Canadian Symposium on Remote Sensing, St. Johns, Newfoundland, pp 327-336.

Gillespie, A.R., A.B. Kahle and F.D. Palluconi, 1984, Mapping alluvial fans in Death Valley using multichannel thermal infrared images, Geophys. Res. Lett. *11*, 1153-1156.

Gillespie, A.R., A.B. Kahle and R.E. Walker, 1986, Color enhancement of highly correlated images: I. Decorrelation and HSI stretches, Remote Sensing of Environment, *in press*.

Kahle, A.B. and L.C. Rowan, 1980, Evaluation of Multispectral Middle Infrared Aicraft Images for Lithologic Mapping in East Tintic Mountains, Utah, Geol., *8*, 234-239.

Kahle, A.B. and R.E. Walker, 1984, Calculation of Emissivity and Thermal Inertia at Death Valley, California, from TIMS Data, Proc. 9th Canadian Symposium on Remote Sensing, St. Johns, Newfoundland, pp 337-346.

Kahle, A.B. and A.F.H. Goetz, 1983, Mineralogic Information From a New Airborne Thermal Multispectral Scanner, Science, 222, 24-27.

Lyon, R.J.P., 1965, Analysis of Rocks by Spectral Infrared Emission (8 to 25 Microns), Econ. Geol., *60*, 715-736.

Palluconi, F.D., and G.R. Meeks, 1985, Thermal Infrared Multispectral Scanner (TIMS): An investigator's guide to TIMS data, JPL Publication *85-32*, Jet Propulsion Laboratory, Calif. Inst. Technology, Pasadena, CA, 22 pp.

Soha, J.M. and A.A. Schwartz, 1978, Multispectral Histogram Normalization Contrast Enhancement, Proc. 5th Canadian Symposium on Remote Sensing, Victoria, B.C., pp 86-93.

Rindfleisch, T.C., J.A. Dunne, H.J. Frieden, W.D. Stromberg, R.M. Ruiz, 1971, Digital processing of the Mariner 6 and 7 pictures, Jour. Geophys. Res., 76, 394-417.

* * * * *

Thermal Imaging Spectroscopy in the Kelso-Baker Region, California.

Philip R. Christensen, Michael C. Malin, Donald L. Anderson, and Linda L. Jaramillo.
Dept. of Geology, Arizona State University, Tempe, AZ. 85287.

The primary objective of our study was to assess the ability of TIMS data to uniquely identify rock composition using thermal-infrared spectroscopy. For this study we selected a region with a wide range of rock and soil types in an arid environment, and compared the spectra acquired by TIMS to laboratory spectra of collected samples. A second objective was to use the TIMS data to study the potential for compositional mapping of Mars, the Moon, and other solar system bodies, in addition to the Earth.

To address these goals, a TIMS image was acquired of the Kelso-Baker region in the Mojave desert of California at a surface resolution of approximately 7 m. The image covers a range of mapped rock compositions, including the Cima volcanic complex, composed of basalt/andesite flows, the quartz-rich Kelso sand dunes, and a suite of carbonates, quartzites, and metamorposed sedimentary rocks in the Kelso mountains, as well as a range of alluvial materials. Each of these components can be readily distinguished based on variations in their spectral properties over the six TIMS bands. We generated a principal component image of the region using bands 1, 3, and 5, and applying the technique described by Kahle and Rowan (1980) and Kahle and Goetz (1983). This image was then used to map the areal extent of each geologic component. These units were compared to existing geologic maps of the area to determine the ability of TIMS to reproduce and improve the mapping capabilities obtained by direct field investigation. This study revealed subtle compositional distinctions not previously mapped and, as has been reported previously (Kahle and Goetz, 1983; Gillespie et al., 1984), the TIMS data in many cases greatly improved the location of geologic contacts and identified small outcrops not previously mapped. Using the unit map derived from the TIMS data, a field reconnaissance was conducted in May, 1985 to investigate the cause of the variations in spectral properties and to collect samples for laboratory analysis.

TIMS Spectral Analysis

Using data from each of the six TIMS bands, spectra of the major units in the area were made. These spectra were generated from data calibrated for instrument response. Each spectral point was determined by averaging over areas three pixels by three pixels in size. Examples of these spectra are shown in Figure 1. Figure 1a gives the data offset in emissivity for clarity; Figure 1b shows the same data plotted with no offset. The emissivity scale is approximate, based on preliminary estimates of surface kinetic temperature.

Field Studies

A variety of surfaces were examined to determine the composition of the rocks present and to study the origin of the units characterized by the TIMS data. The region can be roughly divided into three geologic provinces using the TIMS data alone. These consist of the basalt flows at the north end of the region, the high-silica sand dunes to the south, and the sediments and meta-sediments in the center portion of the study area.

The sand dunes have a very high silica content, as can be seen from the six-point spectra extracted from the original TIMS images (Fig. 1). The spectral character of the dunes varies across the field. However, this variation is due to changes in the depth of the absorption band centered at 9.2 μm, rather than in the position of the band center (Fig. 1). Field investigation revealed that these changes are produced by variations in the abundance

of vegetation, which appears to be essentially blackbody in nature. Therefore, the vegetation reduces the spectral contrast, but does not introduce a second spectral component. Using the TIMS data alone, the active, vegetation free regions of the dunes can be readily distinguished from the inactive regions stabilized by plant cover. Because of the strong differences in the spectral properties of quartz sand and vegetation, TIMS provides a useful tool for remotely distinguishing regions of unvegetated, active sand from regions with low (~10%) plant cover.

The Cima basalt flows in the northern portion of the area appear very uniform in both the TIMS image and the six point spectra (Fig. 1). Even when this area is isolated, a principal component stretch is performed on this region alone does not reveal significant variations. The composition of these flows does not appear to vary significantly throughout the field, consistent with the uniform spectral signature observed by the TIMS data. However, field investigation showed that a wide range of surface textures and particle sizes do occur on these flows. The surfaces observed included fresh, relatively unweathered aa lavas, with up to 1.5 m of surface roughness, as well as smooth, desert pavements composed of basalt fragments that cover up to 90% of the surface, and smooth deposits of 1 to 5 mm cinders. These observations indicate that surface texture does not play an important role in controlling the thermal emission characteristics in this area. This finding has important implications for extrapolation of thermal-IR spectral measurements to other regions and to other planetary surfaces. For this region, composition, rather than texture, controls the observed thermal-IR spectral properties.

These greatest compositional variability occurs in the combined suite of sediments, meta-sediments, and igneous intrusives of the Kelso mountains. Several units are easily distinguished spectrally (Fig. 1), including carbonates and quartzites. Of particular interest is a suite of rocks that have been mapped together as pre-Cambrian metamorphic rocks. This suite is readily separated into different units using the TIMS data. Field investigation of these units revealed them to be a range of silica-rich igneous and metamorphic rocks that had subtle differences in the composition and abundance of mafic and feldspar components. These subtle differences can be identified in hand specimens of the different units, but the distinctions are not simple, nor readily apparent. The increased abundance of mafic minerals in the metamorphic rocks can be seen in the spectra (Fig. 1) as an absorption band near 9.8 μm. The quartz minerals also produce an observable absorption band between 8.8 and 9.2 μm, as can be seen by comparing the spectra of this material to that of the quartz sand dunes. Therefore, it is possible to infer the general composition of these rocks as containing both abundant silica rich and mafic minerals from the TIMS spectra alone, although at present no attempt has been made to estimate the abundance of these components from the TIMS spectra alone.

In summary, the TIMS data provide an excellent means for discriminating and mapping rocks of very similar mineralogy. The spectra obtained from the TIMS data demonstrate the differences in absorption band location and strength between rocks different rock types, and confirm that there are systematic differences. Qualitatively, the spectral character can be used to predict the dominant mineralogy of these rocks. These predictions are confirmed by hand specimen and laboratory spectral analysis. For the rocks in this study area, it is composition, rather than particle size or surface texture, that controls the thermal emission characteristics. These findings suggest that thermal-infrared spectroscopy can provide a powerful tool for identifying and mapping rock composition on the Earth and other terrestrial planets.

References

Gillespie, A.R., A.B. Kahle, and F.D. Palluconi, Mapping alluvial fans in Death Valley, CA, using Multichannel Thermal Infrared Images, Geophys. Res. Letters, 11, 1153-1156, 1984.

Kahle, A.B. and L.C. Rowan, Evaluation of multispectral middle infrared aircraft images for lithologic mapping in the East Tintic Mtns, Utah, Geology, 8, 234-239, 1980.

Kahle, A.B. and A.F.H. Goetz, Mineralogic information from a new airborne thermal infrared multispectral scanner, Science, 222, 24-27, 1983.

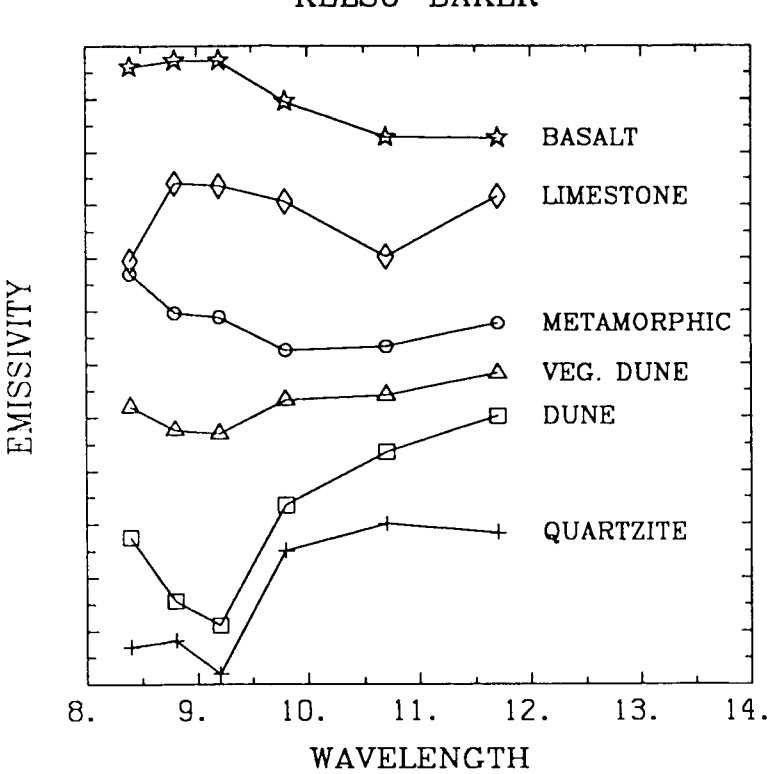

Figure 1a. Six-point spectra extracted from TIMS image of rock units in the Kelso-Baker region, California. Spectra are offset in emissivity for clarity.

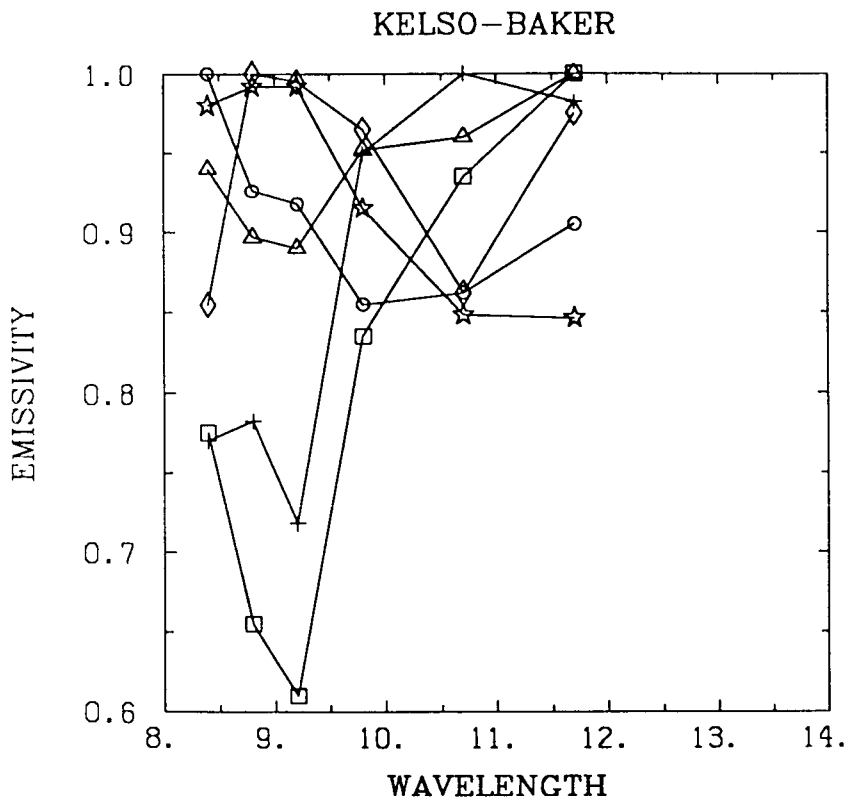

Figure 1b. Same data shown in Figure 1a, but with no offset in emissivity.

LITHOLOGIC MAPPING OF SILICATE ROCKS USING TIMS

A.R. Gillespie

Geology Group
Jet Propulsion Laboratory
California Institute of Technology
Pasadena, California 91109

ABSTRACT

Common rock-forming minerals have thermal infrared spectral features that are measured in the laboratory to infer composition. NASA now operates an airborne Daedalus scanner (TIMS) that collects six channels of thermal infrared radiance data (8 to 12 μm) that may be used to measure these same features for rock identification. Previously, false-color composite pictures made from channels 1,3, and 5 and emittance spectra for small areas on these images have been used to make lithologic maps. In this article, central wavelength, standard deviation and amplitude of normal curves regressed on the emittance spectra are related to compositional information for crystalline igneous silicate rocks. As expected, the central wavelength varies systematically with silica content and with modal quartz content. Standard deviation is less sensitive to compositional changes, but large values may result from mixed rock types within a pixel. Amplitude varies with quartz content and also with admixture of vegetation. Compression of the six TIMS channels to three image channels made from the regressed parameters may be effective in improving geologic mapping from TIMS data, and these synthetic images may form a basis for the remote assessment of rock composition.

INTRODUCTION

Common rock-forming minerals have thermal infrared spectral characteristics that can be used to infer rock compositions and construct lithologic maps from remotely sensed images. The strongest spectral features lie between 8 and 10 μm and are attributed to the fundamental vibrations of Si-O [e.g., Hunt and Salisbury, 1974; Hunt, 1980]. These *reststrahlen* bands are most pronounced in quartz. Partial substitution of Al, Mg or other elements for Si in a wide range of silicate minerals results in changes in the width, depth and wavelength of the band, as well as changes in its fine structure [e.g., Lyon, 1965]. For example, reststrahlen bands for quartz (SiO_2) are centered near 8.6-9.2 μm; for albite ($NaAlSi_2O_3$) at about 8.7-9.9 μm; and for olivine ($(Mg,Fe)_2SiO_4$) at about 10.0-10.5 μm. Although rock spectra are not simple mixtures of mineral spectra, systematic differences in the emittance spectra of rocks do correspond to features in the spectra of the major constituent minerals. These differences are sufficient to produce distinct differences in the apparent temperatures measured remotely, at different wavelengths. Thus multispectral thermal measurements are a means of

assessing rock composition, and multichannel thermal infrared images are a means of extending this information regionally, to form a basis for lithologic maps [e.g., Vincent et al., 1972; Kahle and Rowan, 1980].

Recently, NASA has acquired a Thermal Infrared Multispectral Scanner (TIMS) that measures six channels of photon flux data in the spectral region 8-12 μm [Palluconi and Meeks, 1985]. Previously, TIMS data have been displayed as false-color pictures made from three of the six image channels, enhanced to emphasize emittance information [Soha and Schwartz, 1978; Gillespie et al., 1986]. This approach does not make use of information from the discarded image channels. In a different approach, thermal emittances may be calculated from each of the image channels and displayed as spectra [Kahle and Walker, 1984]. Although in this approach no data are discarded, the obvious advantages of photo-interpretation cannot be exploited because the data are no longer displayed as pictures. If the emittance images themselves are displayed as false-color pictures, then three channels must still be discarded.

This paper discusses a method that combines the virtues of both the pictorial and spectral analyses. I model the calculated emittance spectra with Gaussian functions, which have only three parameters: a central wavelength, a standard deviation, and an amplitude. In principle, these may be displayed using color pictures. Because the displayed parameters are calculated from all six measured values, more information is displayed than in false-color pictures made from the acquired data. In this paper, I attempt to show that significant lithologic information is contained in these calculated parameters, and that they vary systematically with conventional measures of composition. The three parameters thus form a basis for quantitative photo-interpretation and lithologic mapping.

DATA ACQUISITION

TIMS Data

TIMS is a Daedalus airborne line-scanner operated by NASA on its NSTL Lear jet. TIMS acquires six channels of radiance (photon flux) data in spectral bands having peak sensitivities at 8.3, 8.7, 9.1, 9.8, 10.4, and 11.3 μm, respectively. Details of the instrument are available in Palluconi and Meeks [1985].

During the summer of 1982 TIMS was flown over granitic rocks in the Sierra Nevada batholith, California, and again over the Josephine ophiolite in northern California and southern Oregon, acquiring data for a wide range of crystalline igneous silicate rocks. TIMS data acquired over Death Valley, California [Kahle and Walker, 1984] were used to augment these data. TIMS was flown near noon to maximize the thermal radiance and hence the signal/noise ratio. Data were provided to JPL by NASA/NSTL as computer-compatible tapes.

Ancillary Data

Thermal reflectance spectra were measured for representative rock samples collected in the field, on freshly broken and natural weathered surfaces. This was done at JPL using an Analect Fourier Transform Infrared Spectrometer. Spectra were averaged for roughly 25 locations on each rock sample, depending on grain size, to ensure that they represented the bulk rock composition and could be related to TIMS data collected over outcrop areas of ~400 m^2.

Estimates were made of the modal mineral abundances in selected samples by point counts of thin sections [Gillespie and Abbott, 1984]. SiO_2 content was measured by electron microprobe analysis of glass beads fused from powdered rock samples [e.g., Nash, 1964; Baldridge, 1979]. Results were checked against values calculated from the modal mineral abundances for the same samples.

DATA PROCESSING

TIMS Data

Calibration and Correction... The TIMS images were corrected for systematic panoramic distortions using a nearest-neighbor algorithm (not interpolation), to avoid further spectral mixing than was inherent in the data as acquired. The data were converted to units of photon flux, using the line-by-line internal blackbody reference or calibration values. Some additional aspects of required image processing are found in a companion paper [Gillespie, 1986]. After the data were corrected for instrument effects, emittance values were calculated for the six image channels, using a variation of the method of Kahle et al. [1980].

Calculating Emittances From TIMS Data... In order to calculate emittances from TIMS data, it is necessary to assume an emittance for one channel because there are seven unknowns (six emittances and the temperature) but only six radiance measurements. Based on this assumption, a model ground temperature can be calculated for each point in the image. Emittances for the other channels are then found from the measured photon flux ratioed to the flux predicted by Planck's Law for a blackbody at the model temperature. In this way, emittance images for all six channels were constructed from the acquired radiance images.

Kahle et al. [1980] assumed the emittance in channel 6 was always 0.93. This is valid for granites, but not for mafic and ultramafic rocks, which have low emittances near 11 μm. For these rocks the reststrahlen band lies at longer wavelengths than channel 1, and the emittance in channel 1 is more-or-less constant. Therefore, for granitic rocks the assumption of Kahle et al. [1980] was used, but for mafic and ultramafic rocks the

emittance in channel 1 was taken to be 0.98, a value that was measured for several samples on the Analect spectrometer. In the future a more elegant solution would be to calculate the apparent blackbody temperature for each TIMS channel; the channel for which the maximum temperature was found would be assigned an arbitrary emittance (e.g., 0.95), and the remaining emittances would be calculated as described above. It would be useful to create an image that reported the channel which had the maximum temperature, also. For this study, however, the simplified scheme in which either channel 1 or 6 was fixed was used.

Atmospheric Effects... The method of calculating emittances described above does not correct for atmospheric effects such as absorption and radiation by water vapor. While model corrections have been applied [Kahle et al., 1981], these depend on some knowledge of the air mass above the scene at the time of data acquisition. For the images used in this study, that vital information was lacking.

However, recent investigations with JPL's Portable Field Emission Spectrometer have shown that vegetation is spectrally flat in the 8-12 μm region. Any observed structure in the TIMS emittance spectra of vegetation is thus a measure of actual atmospheric effects. Therefore, atmospheric effects were reduced by normalizing the calculated emittances to values found for vegetation in the same scene. This approach is valid for multiplicative mixing (e.g., translucent atmosphere) but not for additive mixing (e.g., radiating atmosphere). It is valid only for a similar optical path through a single air mass; thus the target and the vegetation must be at similar scan angles and elevations, and must be viewed through the same mass of air. Water vapor affects primarily TIMS channel 1, whereas atmospheric ozone affects channel 4. The effect on channel 1 appears to be stronger and more variable than for channel 4.

Ultimately, it will be desirable to correct for both multiplicative and additive atmospheric effects. The iterative spectral mixing models of Adams et al. [1986] could probably be modified to do this. One of their advantages is that it is not necessary to completely describe the atmosphere in order to identify and remove its effects on the image spectra.

Sampling the Image Data... For this study, six-valued emittance spectra were extracted from the processed images for sites identified on an interactive image analysis station at JPL's Image Processing Laboratory. Sites were selected based on field experience and existing geologic maps [Moore, 1963; Cater and Wells, 1953; Harper, 1980, 1984] to represent all major rock types encountered in the scenes studied. They were chosen because they contained outcrops of rock larger than the ~20-m nadir pixels, no vegetation, and little soil.

Laboratory Spectra

Thermal infrared reflectance spectra were also obtained in the laboratory for rock samples collected at some sites identified in the TIMS images. Kahle et al. [1984] have demonstrated that, for remote observations of many natural rock surfaces, emittance and reflectance are strongly anticorrelated at thermal infrared wavelengths, and are in fact related through Kirchoff's Law:

$$\varepsilon(\lambda) = 1 - r(\lambda) \qquad (1)$$

where $\varepsilon(\lambda)$ is the emissivity or emittance and $r(\lambda)$ is the reflectivity or reflectance at wavelength λ [e.g., Lyon, 1965]. Such is not the case for all samples, for example, powders and polished surfaces [Conel, 1969]. I calculated emittance spectra according to equation (1). TIMS emittance values were simulated from laboratory data by integrating the product of the calculated emittance spectra and the TIMS instrument response functions for the six channels.

Data Regression

All TIMS and simulated TIMS six-valued emittance spectra for the selected sites and rock types were fitted by Gaussian functions according to

$$\varepsilon(\lambda) = 1 - \frac{A}{\sqrt{2\pi}} \exp\left[-\frac{1}{2}\left[\frac{\lambda - \lambda_c}{\sigma}\right]^2\right] \qquad (2)$$

where A is the amplitude, λ_c is the central wavelength and σ is the standard deviation. Note that in equation (2) the Gaussian function is actually related to $r(\lambda)$, not $\varepsilon(\lambda)$. The fitting was done by linear regression on the cumulative distribution function of $(1-\varepsilon(\lambda))$ values plotted, on a probability grid, against the peak wavelengths of the six spectral bands of TIMS. The central wavelength λ_c of the fitted function was found from the abscissa (λ) value for which the regressed line had an ordinate value (probability) of 0.5. The standard deviation was found from the difference between λ_c and the wavelength at which the probability was 0.68. The third parameter, the amplitude A of the fitted function, cannot be found in the above manner. Instead, A is taken to be the maximum difference found among the six calculated emittance values.

RESULTS

TIMS and Laboratory Spectra

Figures 1 through 5 show laboratory reflectance spectra and TIMS emittance spectra for fresh and weathered silicate rocks. Laboratory spectra for freshly broken samples are shown in Figure 1, plotted with reflectance increasing downward, to simulate emittance. All the samples came from the study areas, except the Eureka Quartzite, which was from the Death Valley data [Kahle and Walker, 1984]. Reflectances range from 1% to 79% with the maximum value (minimum emittance) occurring at different wavelengths from sample to sample, from 8.6 to 10.3 μm.

The orthoquartzite exhibited the greatest emittance (reflectance) contrast, with a double reststrahlen band from 8 to 9 μm which is characteristic of SiO_2. This doublet is also prominant in the spectrum of the quartz-rich (28%) Bullfrog quartz monzonite, along with other bands attributable to feldspar and possibly clay minerals. These bands are found from 9 to 10 μm, and make the spectrum asymmetric. The maximum reflectance is ~37%, much less than for the Eureka Quartzite. This is probably due to the lower quartz content of the Bullfrog pluton and to the abundance of feldspar, which has less intense reststrahlen bands than quartz.

The spectrum of quartz-poor (7%) rocks, also from the Bullfrog pluton, shows the quartz bands subordinate to the feldspar bands, which have peak reflectances of only 12%. The spectrum of the hornblende diorite, which has only a trace of quartz, has even lower reflectances for $\lambda <$ ~9 μm. The feldspar (plagioclase) band near 9.5 μm is still present, but the largest band is probably due to the hornblende, centered near ~10.2 μm.

Finally, the spectrum of the Josephine Peridotite has an intense band (38% contrast) near 9.5 μm, and a large shoulder near 11 μm. The dominant band is attributable to serpentine minerals; the smaller features are probably due to olivine.

Figure 2 contrasts laboratory reflectance spectra for freshly broken and natural weathered surfaces of the quartz-rich Bullfrog quartz monzonite and the serpentinized Josephine Peridotite of Figure 1. Weathered surfaces of both rock types are less than half as reflective as the fresh surfaces in the reststrahlen bands. Surprisingly, the contrast in quartz bands is reduced proportionately more than the bands at longer wavelengths, for the quartz monzonite. We tentatively attribute this to the presence of a thin clay coat on the weathered surface. Reststrahlen bands for the clay minerals from 9 to 10 μm would keep contrast high there.

Contrast for the weathered peridotite is reduced even more than for the quartz monzonite. A broad feature is still evident at 10 μm, however. Apparently, the serpentine minerals are not preserved on the weathered surface, which consists primarily of Fe oxides, orthopyroxene, and minor olivine.

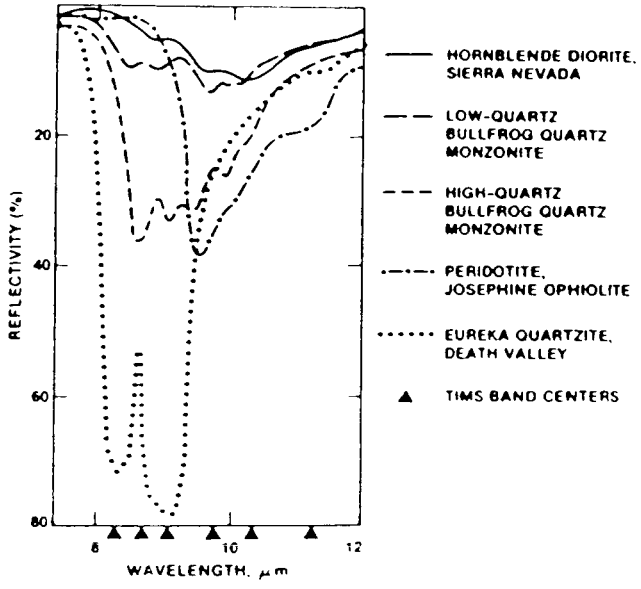

Figure 1. Laboratory reflectance spectra of fresh silicate rocks (reflectance increases downward).

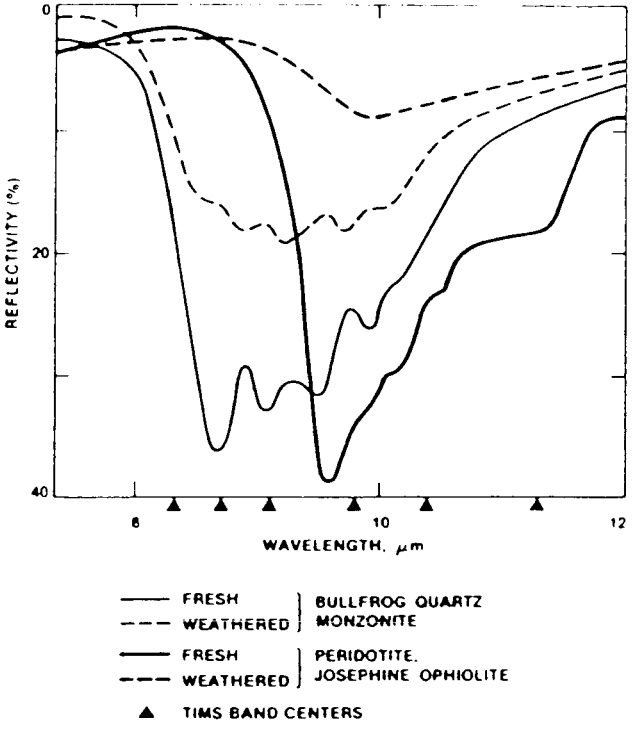

Figure 2. Laboratory reflectance spectra of fresh and weathered rocks

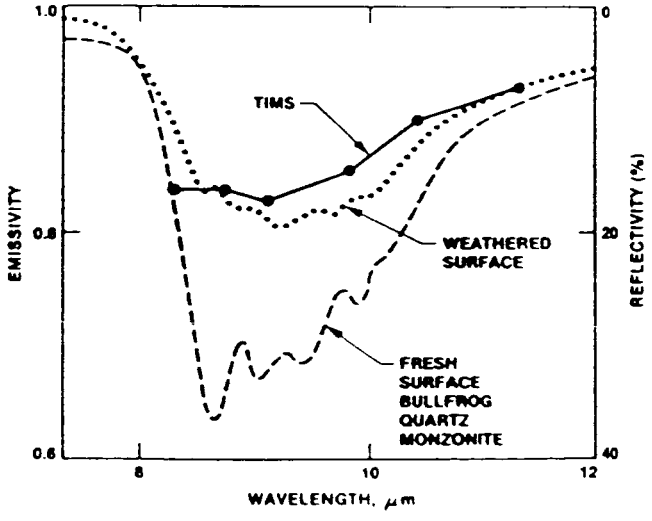

Figure 3. Laboratory reflectance spectra of freshly broken and natural weathered surfaces of Bullfrog quartz monzonite compared to emittance spectra calculated from TIMS

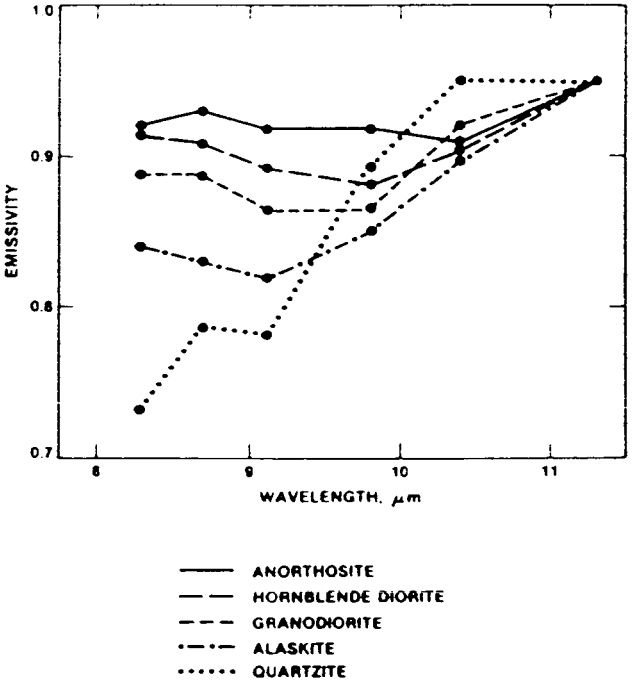

Figure 4. TIMS emittance spectra of silicate rocks ($\varepsilon_\lambda \equiv 0.95$). The quartzite spectrum was not corrected for atmospheric effects.

Figure 2 emphasizes that remotely sensed images show natural surfaces that are not compositionally the same as the fresh bedrock. Nevertheless, weathering is not necessarily so intense that bedrock composition cannot be inferred.

Figure 3 compares the TIMS emittance spectrum for an outcrop of the quartzose facies of the Bullfrog pluton to the laboratory reflectivity spectra of fresh and weathered surfaces. Clearly, the TIMS spectrum does not resemble the spectrum of the fresh surface, but it is similar to the spectrum of the weathered surface. Even so, the emittance for TIMS channel 1 appears to be somewhat too low. Perhaps this is due to incomplete correction for atmospheric water, which affects channel 1 most strongly. It is also possible that the disagreement arises from an incorrect choice of the model emittance for channel 6. To first order, this would introduce a gradient in the apparent spectrum, because of the non-linear nature of the Planck function.

Figure 3 reinforces the findings of Kahle et al. [1984], and demonstrates that TIMS emittances and the laboratory reflectance spectra used in this study are in fact related through Kirchoff's law (equation 1).

Figure 4 presents five TIMS emittance spectra for different silicate rock types. As in Figure 1, the Eureka Quartzite spectrum has the highest contrast. The emittance for TIMS channel 1 is lower than expected from the spectrum of the quartzite, which we attribute to atmospheric water. Kahle and Walker [1984] did not correct the quartzite spectrum for atmospheric effects by the method described here, because of the absence of vegetation in Death Valley. The minimum emittance of 0.22 for the other channels is considerably less than the value of 0.77 predicted by Kirchoff's Law for the fresh quartzite. Perhaps this is due to a thin film of desert varnish of the natural weathered surface. Even so, the quartzite spectrum has more contrast than those for the igneous silicate rocks.

The spectra of the igneous silicate rocks show a decrease in contrast and an increase in the wavelength at which the minimum emittance is found as the composition becomes more mafic, as expected.

Figure 5 shows TIMS emittance spectra for serpentinized Josephine Peridotite and for lateritic soils developed over the peridotite. The soil spectrum is nearly flat, a result corroborated by data from the JPL Portable Field Emission Spectrometer. The peridotite spectra differ from the laterite and from each other primarily in channels 4 and 5 (9.8 and 10.3 μm). In Figure 5 it is evident that a false-color picture of the kind used in most early studies of TIMS data, based on channels 1, 3, and 5, would discriminate between the fresh and weathered rock poorly, because channel 4 was discarded. This emphasizes the need to examine all six image channels in lithologic mapping.

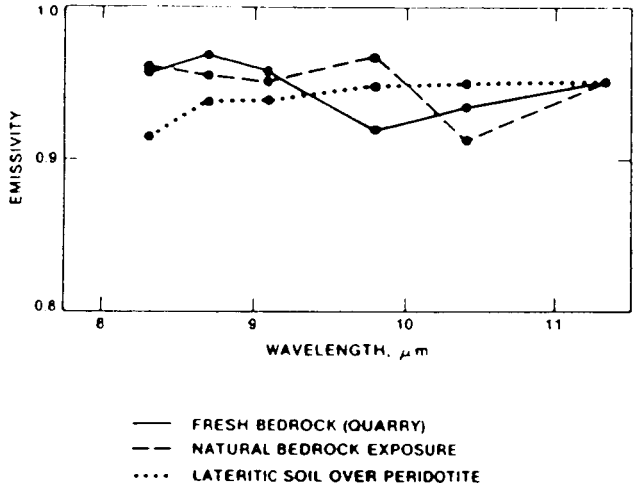

Figure 5. TIMS emittance spectra for Josephine Peridotite and lateritic soils in northern California. The emittance for Channel 6 was set to 0.95 for comparison to Fig. 4.

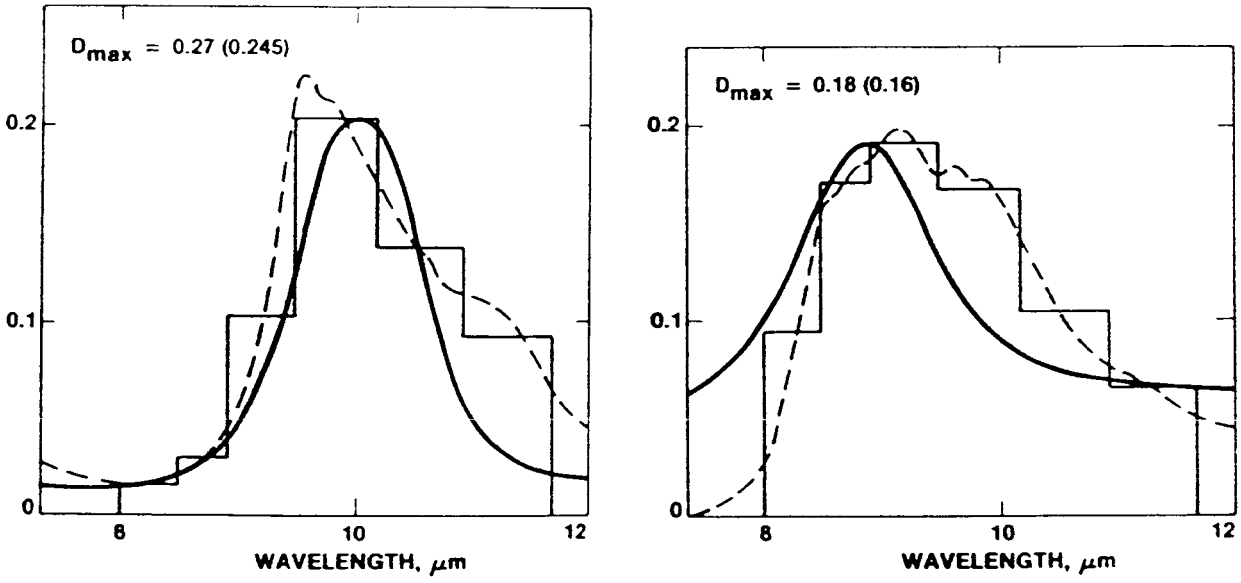

Figure 6. Continuous laboratory reflectance spectra (dashed line), simulated TIMS emittance spectra (light solid line), and Gaussian functions fitted to TIMS spectra (heavy solid line). Left figure is for serpentinized peridotite; right figure is for quartz monzonite. Kolmogorov-Smirnov test statistic is in the upper left-hand corner. Parenthetical values are calculated for reflectance *vs* λ^{-1}.

Figure 5 shows that soils developed atop bedrock need not resemble the unweathered substrate at all. However, it should be possible to discriminate between soil and bedrock, and even to estimate the degree and weathering on bedrock outcrops.

Fitting Gaussian Functions to TIMS Data

Figures 6 through 9 describe the regression of normal functions to the emittance spectra and show the relationship among the three parameters of the fitted curves: **A**, λ_c and σ. Figure 6 shows laboratory reflectance spectra, simulated TIMS data and the curves fitted to them for peridotite and quartz monzonite. For peridotite, the continuous spectrum is simple, and the assumption that it may be fitted by a Gaussian function appears to be realistic. The continuous spectrum for the quartz monzonite contains several distinct features, and will be less well described by a Gaussian function. However, the complexity is not evident in the TIMS spectrum, which is severely undersampled.

The normality of the TIMS spectra was tested with the one-sample Kolmogorov-Smirnov test [e.g., Bradley, 1968; Till, 1974], using the modified tables of Lilliefors [1967] that apply when the population is unknown. The test results show that the hypothesis that the TIMS spectra are normal cannot be rejected at the 80% confidence level. Fitting curves according to wavenumber rather than wavelength did not appreciably improve the fit. The use of normal curves to describe the six-valued TIMS spectra is probably justified, although this might not be true for image data having higher spectral resolution and more channels.

Figure 7 presents a variation diagram relating **A** (emittance contrast) and λ_c (central wavelength) for normal functions fitted to TIMS emittance spectra for various silicate rocks. The data loosely follow a trajectory in this diagram, according to lithology. A general dispersion of rock types with λ_c is more pronounced than with **A**. It appears that **A** decreases as λ_c increases for granitic rocks, but for mafic and ultramafic rocks **A** is unchanged over a 0.6-μm range of λ_c. These results are predictable from the laboratory data presented above. However, the scatter of data - especially along the **A** axis - may arise in part from natural variability of weathered surfaces in the TIMS data. In particular, minor amounts of vegetation, including lichens, will strongly affect **A**.

Figure 8 shows the effect of spectral mixing between bedrock and vegetation (blackbody or graybody spectrum) in TIMS data. The emittance contrast in the spectrum for quartz monzonite is progressively reduced with increasing vegetative cover. This effect is noticeable for as little as 5% cover and profoundly influences the parameter **A**. There appears to be little effect on the shape of the spectra; therefore, we expect σ and λ_c to be less sensitive than **A** to partial vegetation cover.

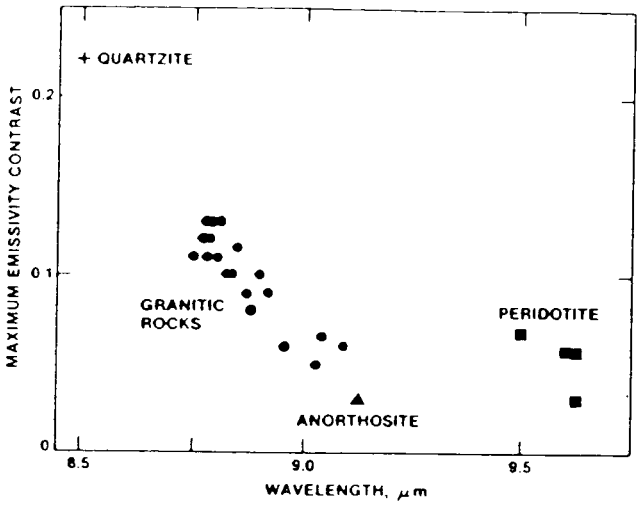

Figure 7. Variation diagram relating A (maximum emittance contrast) and λ_c (central wavelength) for TIMS emittance spectra for various silicate rocks.

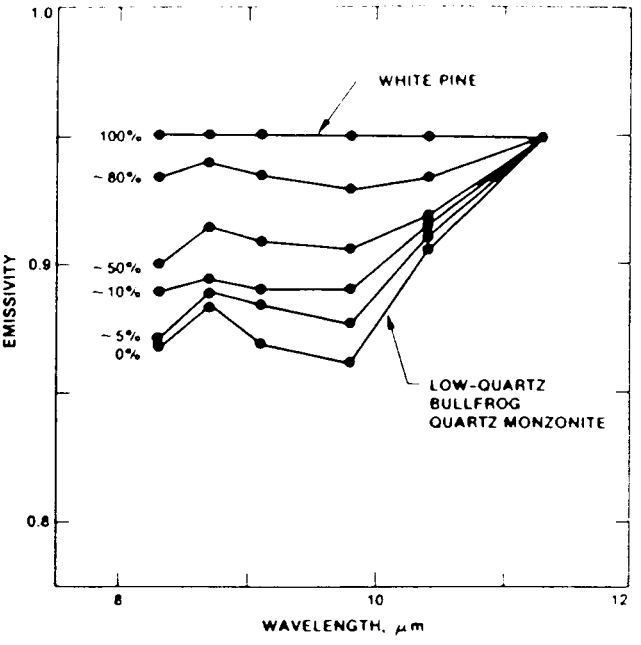

Figure 8. TIMS emittance spectra for rocks of the Bullfrog pluton (Sierra Nevada) under partial vegetation cover (shown to the left of the spectra).

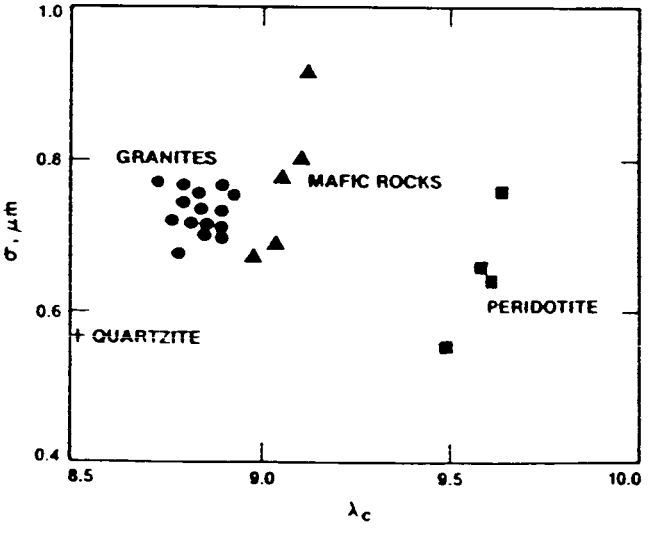

Figure 9. Variation diagram relating regression parameters σ (standard deviation) and λ_c for TIMS emittance spectra of various silicate rocks.

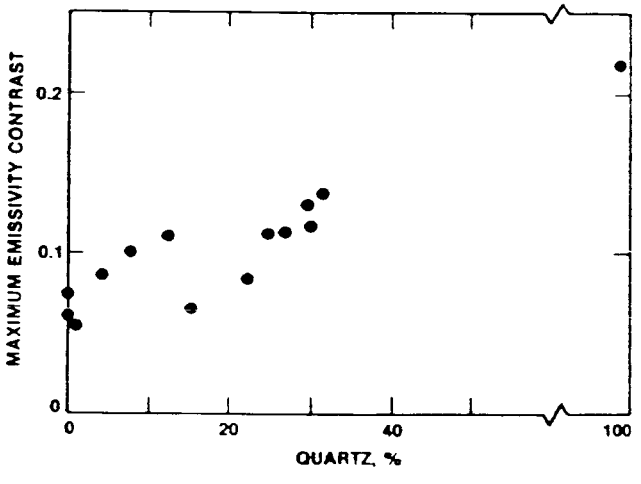

Figure 10. Variation in A (maximum emittance contrast) with modal quartz in simulated TIMS spectra of various silicate rocks, calculated from laboratory reflectance spectra.

It is important to recognize that, in general, spectral mixing in thermal IR images can be quite complicated, even if it is limited to binary mixing between only two endmembers or components. Not only do the emittance spectra characteristic of the endmembers radiating to the sensor differ, but the temperatures at which they radiate may also. Because of the exponential temperature dependence of radiance in Planck's Law, the effect of temperature differences can be profound. At the least, it implies that a particular mixed spectrum can be achieved by quite a range of endmember concentrations or fractions. Further complications are introduced because the shape of the blackbody spectrum is also temperature-dependent. Thus it is non-trivial to estimate the fraction of vegetation cover, for example, from thermal infrared data. Despite this, Figure 8 demonstrates that it is possible to *detect* the presence of mixing in a straightforward manner.

Figure 9 shows the relationship between the regression parameters σ and λ_c for various silicate rocks. Although σ ranges from 0.6 to 0.9, there is no obvious correlation with λ_c. We note that σ is smallest for the monomineralic quartzite and for one of the peridotite samples. Granitic and especially mafic rocks have larger values of σ. Probably σ is larger for rocks containing several minerals, and hence for complicated spectra containing reststrahlen bands at two or more wavelengths. Thus σ, like **A**, may be sensitive to spectral mixing.

Regression Parameters and Rock Composition

Figures 10 through 12 show how the parameters **A** and λ_c vary with two conventional measures of rock composition: modal quartz and silica abundance. Figure 10 relates **A** and modal quartz abundance. As suggested from Figure 7, there is a pronounced positive correlation. The value of **A** ranges from ~0.07 for rocks with no quartz to ~0.16 for granitic rocks with 30% quartz. For the Eureka Quartzite, **A** is 0.22. The parameter **A** is clearly controlled in part by the intense quartz reststrahlen bands. As seen in Figure 8, in most image data **A** will also be controlled by vegetative cover, thus complicating its interpretation.

Figure 11 illustrates the covariation of λ_c and modal quartz. λ_c decreases from 9.7 to 8.5 μm as quartz content rises from 0 to 100%. Half that variation occurs for quartz-free rock types. Ultramafic, mafic and granitic rocks and quartzite are all separable by λ_c. The discrimination of the peridotites and quartz-free diorites shows that λ_c is not sensitive to quartz alone.

Figure 12 illustrates the correlation of λ_c and silica abundance for the same rock types as Figure 11. It is important to emphasize that λ_c is not responding to silica content *per se*; rather, it is responding to the succession of minerals that occurs with increasing silica in igneous rocks. Low-silica rocks contain olivine and pyroxene, both of which have reststrahlen bands near 10 μm. Rocks with more silica contain amphibole and feldspar,

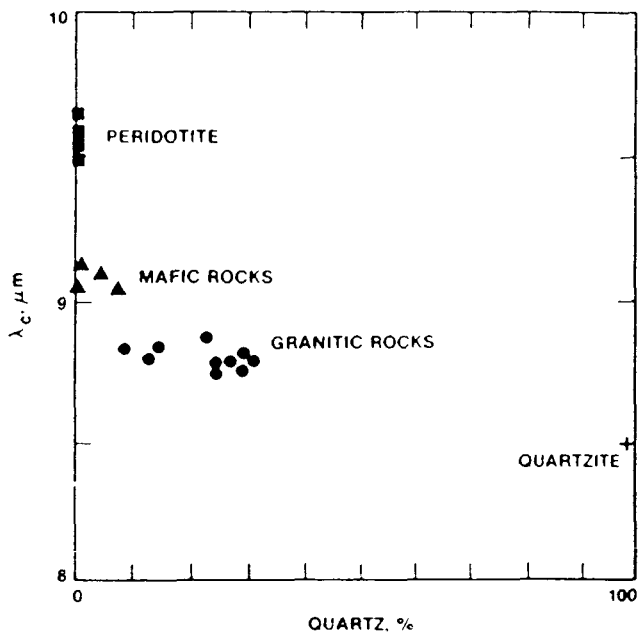

Figure 11. Variation in λ_c (central wavelength) with modal quartz for TIMS emittance spectra of various silicate rocks.

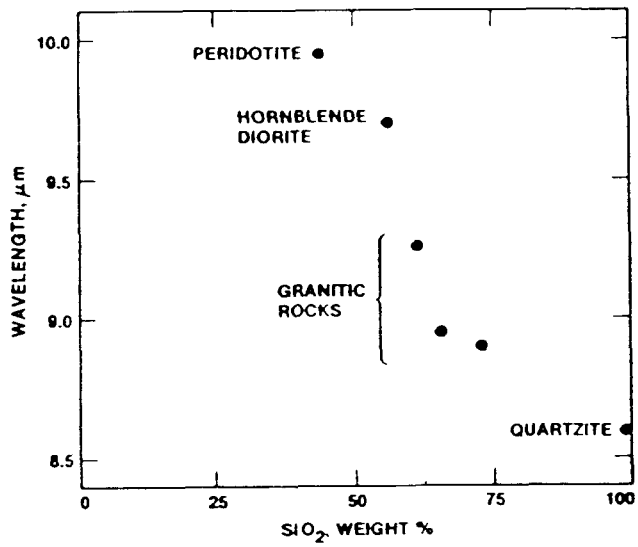

Figure 12. Variation in λ_c (central wavelength) with silica content for simulated TIMS spectra of various silicate rocks, calculated from laboratory reflectance spectra.

which have bands from 9 to 10 μm. High-silica rocks have feldspar and quartz which has bands from 8 to 9 μm. Because silica content is a basis for the classification of igneous rocks, it is useful to note the indirect correlation of λ_c and silica abundance.

The simple relationship between λ_c and modal quartz or silica and the separability of common igneous rock types establishes regression of normal or other appropriate functions on TIMS emittance spectra as a useful tool for the construction of images for photointerpretation. In particular, strong inferences about rock type can be made from λ_c, so images of λ_c will be an aid in lithologic mapping. Addition of A and σ images, along with λ_c, as elements in false-color pictures would increase the amount of information available to the photointerpreter.

SUMMARY

Six-channel emittance images were calculated from radiance images acquired in the spectral region 8-12 μm by the NASA airborne Thermal Multispectral Infrared Scanner (TIMS) over the Sierra Nevada batholith and over the Josephine ophiolite in California. The apparent emittances were fitted by Gaussian functions

intended to model the reststrahlen bands in the emittance spectra. Thus the information contained in the original six-channel image was, in a sense, "compressed" to three channels representing the width, amplitude, and central wavelength of the Gaussian function. The width was greater for multimineralic rocks and appeared to be sensitive to mixing of mineral or rock types. Contrast was especially sensitive to quartz content. The central wavelength was correlated to modal quartz abundances found from thin sections and to silica abundances measured by microprobe analyses of rock samples from selected outcrops representing a range of rock types. It was the best single measure of rock composition. Peridotites, hornblende diorites, granodiorites and quartz monzonites were all separable by the regression parameters.

Vegetative cover as low as 5% influenced the apparent emittances, and especially the contrast in the spectrum. Yet, because vegetation radiates like a blackbody or a graybody, spectral mixing of radiation from vegetation and a substrate does not generally obscure features of the emittance spectrum of the substrate, except for contrast.

Thermal image data appear to be a valuable adjunct to field techniques in geologic mapping of silicate rocks. They augment aerial photographs and near-infrared images in that they depict differences in silicate minerals composing the rocks, not just in the color index, the degree of oxidation, or the extent of hydration.

ACKNOWLEDGEMENTS

NSTL personnel, particularly G. Meeks, have been unstinting in their support, operation, and improvement of TIMS. E. Abbott did the thin section analyses. The research described in this paper was carried out at the Jet Propulsion Laboratory of the California Institute of Technology and sponsored by the Earth Processes Branch of the National Aeronautics and Space Administration.

REFERENCES CITED

Adams, J.B., M.O. Smith and P.E. Johnson, 1986, Viking Lander I: A new map of rock and soil types, Jour. Geophys. Res., *in press*.

Baldridge, W.S., 1979, Petrology and Petrogenesis of Basaltic Rocks and Their Inclusions: Studies from the Rio Grande Rift, the Roman Comagmatic Province, and Mare Procellarum, Ph.D. Thesis, California Institute of Technology, 324 pp.

Bradley, J.V., 1968, Distribution-Free Statistical Tests, Prentice-Hall, Englewood Cliffs, New Jersey, 388 pp.

Cater, F.W. Jr. and F.G. Wells, 1953, Geology and Mineral Resources of the Gasquet Quadrangle, California - Oregon, Geological Survey Bull. 995-C, 133 pp.

Conel, J., 1969, Infrared Emissivities of Silicates: Experimental Results and a Cloudy Atmosphere Model of Spectral Emission from Condensed Particulate Mediums, Jour. Geophys. Res., 74, 1614-1634.

Gillespie, A.R., 1986, Enhancement of TIMS images for photointerpretation, *this volume*.

Gillespie, A.R., and E.A. Abbott, 1984, Mapping compositional differences in silicate rocks with six-channel thermal images, Proc. 9th Canadian Symposium on Remote Sensing, St. John's, Newfoundland, Aug., 327-336.

Gillespie, A.R., A.B. Kahle and R.E. Walker, 1986, Color enhancement of highly correlated images: I. Decorrelation and HSI stretches, Remote Sensing of Environment, *in press*.

Harper, G.D., 1980, The Josephine Ophiolite - Remains of a Late Jurassic Marginal Basin in Northwestern California, Geology, 8, 333-337.

Harper, G.D., 1984, The Josephine Ophiolite, Northwestern California, Geol. Am. Soc. Bull., 95, 1009-1026.

Hunt, G.R., 1980, Electromagnetic Radiation: the Communication Link in Remote Sensing, *in* Siegal, B.S., and A.R. Gillespie, *eds.*, Remote Sensing in Geology, Wiley, New York, pp 5-45.

Hunt, G.R. and J.W. Salisbury, 1974, Mid-Infrared Spectral Behavior of Igneous Rocks, Air Force Cambridge Lab. Tech. Rept. (AFCRL-TR-74-0625.)

Kahle, A.B. and L.C. Rowan, 1980, Evaluation of Multispectral Middle Infrared Aicraft Images for Lithologic Mapping in East Tintic Mountains, Utah, Geol., 8, 234-239.

Kahle, A.B., and R.E. Walker, 1984, Calculation of emissivity and thermal inertia at Death Valley, California, from TIMS data, Proc. 9th Canadian Symposium on Remote Sensing, St. John's, Newfoundland, Aug., 337-346.

Kahle, A.B., D.P. Madura and J.M. Soha, 1980, Middle Infrared Multispectral Aircraft Scanner Data: Analysis for Geological Applications, Appl. Optics, 19, 2279-2290.

Kahle, A.B., J.P. Schieldge, M.J. Abrams, R.E. Alley and C.J. Levine, 1981, Geologic Application of Thermal Inertia Imaging Using HCMM Data, JPL Publication 81-55, 199 pp.

Kahle, A.B., M.S. Shumate and D.B. Nash, 1984, Active Airborne Infrared Laser System for Identification of Surface Rocks and Minerals, Geophys. Res. Lett., 11, 1149-1152.

Lilliefors, H.W., 1967, On the Kolmogorov-Smirnov Test for Normality with Mean and Variance Unknown, Jour. Amer. Stat. Assn., 62, 399-402.

Lyon, R.J.P., 1965, Analysis of Rocks by Spectral Infrared Emission (8 to 25 Microns), Econ. Geol., *60*, 715-736.

Moore, J.G., 1963, Geology of the Mount Pinchot Quadrangle, Southern Sierra Nevada, California, U.S. Geol. Survey Bull. *1130*, 152 pp.

Nash, D.B., 1964, New Technique for Quantitative SiO_2 Determinations of Silicate Materials by X-Ray Diffraction Analysis of Glass, *in* Mueller, W.M., G.R. Mallett and M.J. Fay, *eds.*, Advances in X-Ray Analysis, 7, Plenum Press, New York, pp 209-228.

Palluconi, F.D., and G.R. Meeks, 1985, Thermal Infrared Multispectral Scanner (TIMS): An investigator's guide to TIMS data, JPL Publication 85-32, Jet Propulsion Laboratory, Calif. Inst. Technology, Pasadena, CA, 22 pp.

Soha, J.M. and A.A. Schwartz, 1978, Multispectral Histogram Normalization Contrast Enhancement, Proc. 5th Canadian Symposium on Remote Sensing, Victoria, B.C., pp 86-93.

Till, R., 1974, Statistical Methods For The Earth Scientist, Wiley, New York, 154 pp.

Vincent, R.K., F. Thomson and K. Watson, 1972, Recognition of Exposed Quartz Sand and Sandstone by Two-Channel Infrared Imagery, Jour. Geophys. Res., 77, 2473-2477.

* * * * *

DETECTION AND MAPPING OF VOLCANIC ROCK ASSEMBLAGES AND ASSOCIATED HYDROTHERMAL ALTERATION WITH THERMAL INFRARED MULTIBAND SCANNER (TIMS) DATA COMSTOCK LODE MINING DISTRICT, VIRGINIA CITY, NEVADA

James V. Taranik
Amy Hutsinpiller
Marcus Borengasser

Department of Geological Sciences
Mackay School of Mines
University of Nevada-Reno

Summary

Thermal Infrared Multiband Scanner data were acquired over the Virginia City area on September 12, 1984. The Virginia City area is located in west-central Nevada about 20 miles south of Reno. The highest peak in the area is Mount Davidson which has an elevation of 7,850 feet. The surrounding Washoe and Carson valleys have elevations of 4,500 feet. The flight altitude above mean terrain was 20,000 feet. The data were acquired at approximately 1130 hours local time (1723 IRIG). There is approximately 40% vegetation cover in the area consisting of mostly juniper, sage and grasses.. The area is dominated by an assemblage of volcanic rocks that range in age from Tertiary to Quaternary. These volcanic rock assemblages also contain fluvial and lacustrine sediments of similar age. Unaltered volcanic rocks range in composition from andesite to rhyodacite and their percent silica by weight ranges from 55% to 65%. The volcanic rocks contain very little free quartz. Pre-Tertiary rock units consist of regionally metamorphosed sedimentary and volcanic rocks that have been folded and intruded by granitic rocks. The volcanic rock assemblages have been subjected to intense hydrothermal alteration that has produced secondary quartz, opal, and clay (Thompson, 1956). The historic Comstock Lode District is centrally located in the study area and it produced over 8 million ounces of gold and almost 200 million ounces of silver.

TIMS data have been analyzed using both photointerpretative and digital processing techniques. The Jet Propulsion Laboratory produced enhanced color images using a decorrelation contrast stretch technique. The color negatives were printed at 1:50,000 scale for field use. A VAX11/780 IDIMS image analysis system was used to analyze specific areas at 512 by 512 image resolution. Karhuen-Loeve transformations were utilized to display variations in radiant spectral emittance. The TIMS image data were compared with color infrared metric camera photography, Landsat TM data and key areas were photographed in the field. Only the south-eastern portion of the area has been field-checked in a reconnissance manner.

The Virginia Range consists mainly of intermediate composition flows, breccias, and tuffs of Miocene age. Rhyodacite is most common, however, basalt, rhyolite, and tuffaceous sedimentary rocks of Miocene and Pliocene age cover large areas. Mesozoic metasedimentary and metavolcanic rocks are exposed in places, mostly along the southern and eastern margins of the range. Mesozoic granite and Tertiary diorite and andesite porphyry intrude the younger metamorphic and volcanic rocks. Some domes of extrusive pumiceous rhyolite are present in the area.

Major structures in the Virgin City area are north-trending faults that show evidence of both normal and strike-slip movement (Hudson, 1984). A major east-west trending alignment of drainage intersects the north trending structures and this lineament could be related to a deep seated fracture system which controlled the development of the volcanic pile in the Virginia City area and also the development of Steamboat Springs in Washoe Valley. These structural controls provided the conduits for hydrothermal fluids which have altered the volcanic rock assemblages, and have in some instances facilitated the emplacement of mineralization.

The most recent study of hydrothermal alteration mineral assemblages at Virginia City was done by Hudson (1984). He defines seven major alteration types:

1. Propylitic Alteration: chlorite + albite +/- epidote +/- calcite +/- white mica (illite, montmorillonite, or mixed layered illite-montmorillinite) +/- quartz +/- actinolite

2. Illite-Montmorillinite Alteration: illite + montmorillonite + mixed-layered illite-montmorillonite + quartz

3. Kaolinitic Alteration: kaolinite + quartz

4. Alsic Alteration: Pyrophyllite + quartz + kaolinite +/- diaspore

5. Alunitic Alteration: alunite + quartz +/- diaspore

6. Silicification: quartz

7. Sericitic Alteration: sericite + quartz

Propylitic alteration is the most widespread alteration type. Sericitic alteration is confined to the western portion of the Virginia City area and it is often associated with stockwork quartz veins. Small zones of alunitic alteration are usually surrounded by kaolinitic and/or alsic alteration which in turn are surrounded by illite-montmorillonite alteration. Silification and stockwork quartz veining are structually controlled and are associated with sulfide mineralization (Hutsinpiller, 1985).

Unaltered andesitic rocks of the Alta formation and Kate Peak formation that have approximately 40% vegetative cover appear green on the imagery. Extensive propylitic alteration of these rocks appears to have a dark purple color. Argillic alteration and silicic alteration ranges in color from pink to dark red. Presence or absence of vegetation over altered rock units plays an important role in the degree to which colors, other than green, are displayed. In fact, where brush fires have occurred bright red colors are often displayed by the imagery, but the rocks are only slightly altered and contain little silica by weight percent. A large intrusive plug of biotite-hornblende andesite porphyry with a glassy groundmass (Sugarloaf) is largely unvegetated and appears dark purple on the imagery. Similar rocks having at least 40% vegetative cover appear green. An intrusive dome of Steamboat Hills rhyolite appears bright red on the slope facing the sun and light green on the slope facing away. Vegetative cover is more dense on the north-facing slope of this circular dome, but its composition does not change appreciably.

References

Hudson, D. M., 1984, Geology of the Comstock District, Story County Nevada: Unpublished manuscript, Mackay School of Mines.

Hutsinpiller, A., 1985, High-spectral resolution airborne spectroradiometer data used to define hydrothermal alteration in the Virginia Range, Nevada: Unpublished manuscript, Mackay School of Mines.

Thompson, G. A., 1956, Geology of the Virginia City Quadrangle, Nevada: Geol. Survey Bulletin 1042-C, 77p.

Presented at: TIMS User's Workshop, National Space Technology Laboratories, Bay St. Louis, Mississippi, June 18-20, 1985, sponsored by Jet Propulsion Laboratory, 4800 Oak Grove Drive, Pasadena, California 91109.

Simulation modeling and preliminary analysis of TIMS data from the Carlin area and the northern Grapevine Mountains,Nevada.

Ken Watson, Susanne Hummer-Miller and Fred A. Kruse
U.S. Geological Survey
PO Box 25046, MS 964
Denver, CO 80225

A theoretical radiance model has been employed together with laboratory data on a suite of igneous rocks to evaluate various algorithms for processing Thermal Infrared Multispectral Scanner (TIMS) data. The algorithms tested were two methods based, respectively on principal component(PC) and Munsell transformation decorrelations; a third method based on assuming unit emissivity in TIMS band 6; and a fourth method derived for this study. The fourth method is based on two assumptions: the ground emissivity is temporally invariant and the diurnal temperature change of the atmosphere is small compared to that of the ground. We recognize that testing these methods using the radiance model will always provide a more optimistic result (and thus an upper bound) than can be achieved in nature owing to the simplicity of assumptions about the instrument, the atmosphere, the ground radiation, mixing effects, etc.

We are currently examining two aspects of the general problem. The first is how to extract emissivity information from the observed TIMS radiance data. Simulation tests indicate that the decorrelation models are useful in an approximate way but often merge band-depth and band-position effects. The second aspect is how to use emissivity data in a way that is geologically meaningful. It has been previously reported that for a suite of igneous rocks the emission minima progresses to longer wavelengths as the composition changes from felsic to mafic. Our attempts to correlate emissivity values that correspond to the TIMS bands indicate only a very general correlation with percent silica . The only statistically distinct categories were pure quartz, felsic to intermediate, mafic, ultramafic, and non-silicate.

The four algorithms were evaluated for appropriate band combinations of TIMS data acquired on both day and night overflights of the Tuscarora Mountains, including the Carlin gold deposit, in north-central Nevada. In addition to those areas where mining activity is taking place, only the Eureka Quartzite and part of a jasperoid unit were obviously distinguishable on the processed images. Subtle differences were observed within parts of the carbonate units and the surficial materials, but these did not coincide with mapped unit boundaries. Moreover, a quartzite unit was not distinguishable from surrounding cherts and siliceous shales, possibly due to vegetation cover. The day and night decorrelation images were somewhat similar; however, sufficient color differences could be observed to indicate that these images show differences that are inconsistent with our expectation that the emissivity of the ground is constant in time.

Analysis of a color composited PC decorrelated image (Bands 3,4,5--blue/green/red) of the Northern Grapevine Mountains,Nevada., area showed some useful correlations with the regional geology. Felsic volcanic rocks appear red, a quartz monzonite stock is dark green, and a coarse grained granite appears light blue-green. A small quartz stockwork outcrop can

also be detected on both this and the corresponding Munsell decorrelated image. Color variations in alluvial gravels can be related to different parent rock types.

The thermal infrared region provides fundamental spectral information that can be used to discriminate the major rock types occurring on the earth's surface. These preliminary results using TIMS data indicate that spectral emission differences associated with high silica content can be detected on decorrelated TIMS images, but that optimum use of the thermal infrared region will require appropriate methods of analysis, additional spectral bands, and day and night data acquisition.

N87-17121

APPLICATION OF TIMS DATA IN STRATIGRAPHIC ANALYSIS

H.R. Lang, Jet Propulsion Laboratory, California Institute of Technology*, Pasadena, California 91109.

SUMMARY

An in-progress study demonstrates the utility of TIMS data for unraveling the stratigraphic sequence of a western interior, North American foreland basin. TIMS data can be used to determine the stratigraphic distribution of minerals that are diagnostic of specific depositional environments. TIMS data identify carbonate, gypsum, and quartz-bearing beds in a Permian - Cretaceous sequence. Combined TIMS, and TM results illustrate the feasibility of "spectral stratigraphy", remote lithostratigraphic analysis.

Laboratory transmission spectra reported by Hunt and Salisbury (1975) and Hunt (1980) demonstrated that multispectral thermal data potentially could be used to identify minerals of lithostratigraphic significance (Figure 1). With the availability of TIMS data in 1982, the validity of these laboratory results for geological remote sensing in sedimentary terrane could be tested.

TM and TIMS data were acquired in the Wind River/Bighorn area of central Wyoming in November 1982, and July 1983, respectively. Combined image processing, photogeologic, and spectral analysis methods were used to: 1) map strata, 1) construct stratigraphic columns, 3) correlate strata, and 4) identify mineralogical facies.

Photogeologic interpretation of a 1:250,000 scale TM color composite image identified an appropriate locality for constructing an image-derived stratigraphic column. This "type locality" encompasses exposures of homoclinal strata in the Deadman Butte area of the Casper Arch, eastern Wind River Basin. A 1:24,000 512x512 pixel TM image of the Deadman Butte area provided a photogeologic base for mapping spectral, textural, and geomorphically defined stratigraphic horizons. The TM image geometrically matched USGS 7 1/2' topographic maps. Thus, standard geologic map interpretation methods were used to construct a stratigraphic column incorporating TM spectral characteristics, true stratigraphic thickness and resistance of the photogeologic units. This column was correlated with a conventional surface section measured 10km to the west. Thus, 38 image units were assigned to 11 formations ranging from the Permian Phosphoria to the Cretaceous Cody Shale. The stratigraphic column was also correlated with a similarly constructed column from a structurally complex area in the southern Bighorn Basin and also with well logs from both the Wind River and Bighorn Basin.

*Performed under contract with NASA.

TIMS data were registered to the 1:24,000 scale Deadman Butte TM image. Photogeologic interpretation of a band 1 (blue), 3 (green), 5 (red) decorrelation stretch image of the registered TIMS data provided compositional information for TM defined stratigraphic units. Kahle and Rowan (1980) and Gillespie and others (1984) demonstrated the spectral significance of image colors in similarly processed TIMS data. Red colors in the TIMS Deadman Butte image portray the stratigraphic distribution of quartz (sandstones throughout the section); green, carbonate (dolostones in the Phosphoria Formation and limestones in the Alcova and Sundance Formation); and yellow/green, gypsum (evaporites in the Dinwoody/Red Peak Formation transition). This lithostratigraphic information was incorporated into the TM defined stratigraphic column.

Field sampling sites, selected to represent distinct spectral classes, were identified based upon the TIMS interpretation. In July,1984, these sites were visited and 67 field emission spectra were acquired at 8 field sampling sites with JPL's PFES (see Bartholomew, these proceedings for a description of JPL's field and laboratory thermal spectrometers). Samples were also obtained for laboratory XRD and thermal reflectance analyses. Field and laboratory results confirmed the spectral and compostional interpretation of the TIMS decorrelation stretch image. Four examples of field and laboratory spectral results are illustrated in Figure 2. These results confirm the utility of spectra reported by Hunt and Salisbury (Figure 1) for interpreting TIMS data and support the approach to interpreting colors of band 1,3,5 decorrelation stretch TIMS images cited above. The similarity of field and laboratory spectra illustrated in Figure 2 indicates that laboratory reflectance spectra may be valid surrogates for field spectra in studies of the spectral characteristics of similar rocks in TIMS wavelengths. Additionally these spectra indicate that TIMS ratio images may be useful for mapping sedimentary rocks.

These results demonstrate the feasibility of using coregistered TIMS, TM and topographic data for lithostratigraphic analysis. When available, STIMS data could provide images with sufficient cartographic fidelity to replace TM data as a photogeologic base for similar spectral stratigraphic studies.

REFERENCES

Gillespie, A.R., A.B. Kahle and F.D. Palluconi, 1984, Mapping alluvial fans in Death Valley, California, using multichannel thermal infrared images: Geophysical Research Letters, v.11, p.1153-1156.

Hunt, G.R., 1980, Electromagnetic radiation: the communication link in remote sensing: in, Siegal, B.S. and A.R. Gillespie (eds), Remote sensing in geology, John Wiley & Sons, New York, p.5-45.

Hunt, G.R. and J.W. Salisbury, 1975, Mid-infrared spectral behavior of sedimentary rocks: Environmental Research Papers n.520, Air Force Cambridge Research Laboratories, Hanson AFB, Massachusetts, 49 p.

Kahle, A.B. and L.C. Rowan, 1980, Evaluation of multispectral middle infrared aircraft images for lithologic mapping in the East Tintic Mountains, Utah: Geology, v.8, p.234-239.

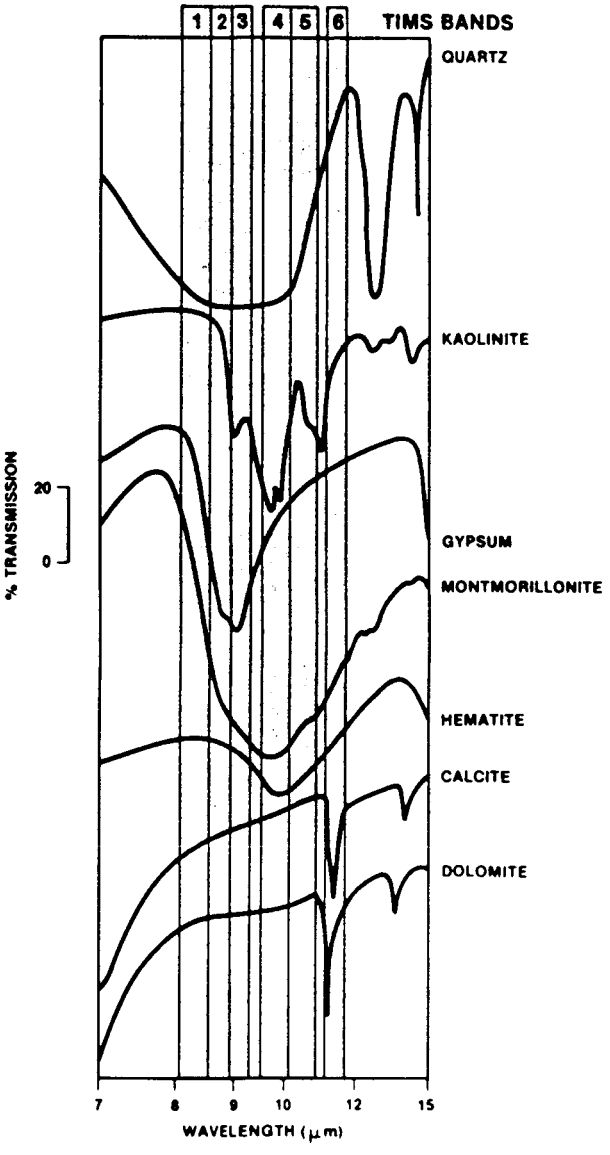

Figure 1. Laboratory transmission spectra of sedimentary rock forming mineral powders (After Hunt and Salisbury,1975 and Hunt 1980).

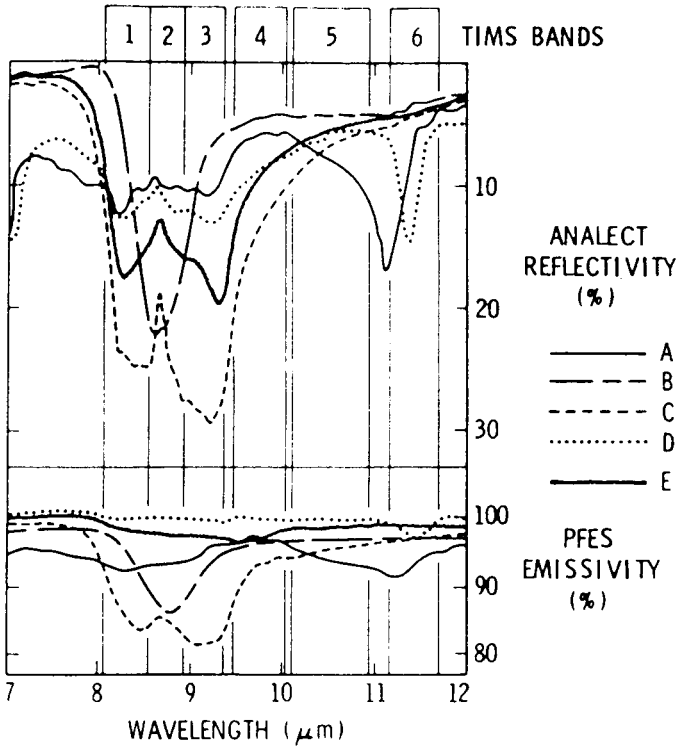

Figure 2. Laboratory reflectivity and field emissivity spectra of the same natural rock surfaces from the Deadman Butte area:
A - dolostone
B - bedded gypsum
C - orthoquartzite
D - marly limestone
E - bentonitic shale.

MONITORING VEGETATION RECOVERY PATTERNS ON MOUNT ST. HELENS USING THERMAL INFRARED MULTISPECTRAL DATA

Kenneth J. Langran
Earth Resources Laboratory
National Space Technology Laboratories
NSTL, Mississippi 39529

INTRODUCTION

The Mount St. Helens 1980 eruption offers a unique opportunity to study vegetation recovery rates and patterns in a perturbed ecosystem. The eruptions of Mount St. Helens created new surfaces by stripping and implacing large volumes of eroded material and depositing tephra in the blast area and on the flanks of the mountain. Areas of major disturbance are those in the blast zone that were subject to debris avalanche, pyroclastic flows, mudflows, and blowdown and scorched timber; and those outside the blast zone that received extensive tephra deposits.

It has been observed that during maximum daytime solar heating, surface temperatures of vegetated areas are cooler than surrounding nonvegetated areas, and that surface temperature varies with percent vegetation cover. This study investigates a method of measuring the relationship between effective radiant temperature (ERT) and percent vegetation cover in the thermal IR (8-12 micron) region of the electromagnetic spectrum.

TEST SITES AND DATA SELECTION

Two test sites were selected as training areas for this study. Test Site A is in the Tephra Deposition Zone approximately 4 miles from the crater and on the south flank of the mountain. This area received extensive tephra deposition from four eruptions subsequent to the initial May 18th eruption. The vegetation in the area of Test Site A is comprised of old growth silver fir stands (Abies amabilis) and clearcuts at varying stages of regrowth. Test Site B is an extended area approximately 7 miles north of the crater in the Tree Blowdown Zone between Cold Water Creek and St. Helens Lake. This area received the full effect of the May 18th eruption.

Vegetation regrowth in the blowdown zone has not been uniform, but controlled by biological and physiographic factors. These include: presence of survivors, moisture availability, deposition level, topographic features, and surface stability. This study and others have observed that vegetation regrowth is highest in pre-eruption clearcuts and alpine meadows, and uniformly low in the blowdown forest (Adams, 1982; Means, 1982). Blowdown areas with snowpack had significantly higher vegetation cover than blowdown areas without snowpack. Regrowth in clearcut areas includes a variety of grasses and herbaceous plants dominated by fireweed (Epilobium augustifolium), Canada thistle (Cirsium arvense), blackberry (Rubus spp.), and other species.

TIMS data was acquired over Mount St. Helens on July 29, 1983 between 1210-1230 hours P.S.T. at an average ground resolution of 12 meters. Color infrared aerial photography was collected concurrently with the scanner data. As a result of excellent atmospheric conditions and minimum air turbulence, the photographic and scanner imagery are of high quality. The data, however, were collected as a functional test of the TIMS and not as part of an ongoing research project; therefore, no concurrent ground verification was conducted during the overflight.

In lieu of collecting field data during the overflight, conventional retrospective ground coverage was substituted. At Test Site A, vegetation type and percent vegetation cover was obtained from the U.S.D.A. Forest Management Data Base System.

The data base, updated annually, identifies information about vegetation and land management activities for each site. Discrete vegetation areas in Test Site B were identified using 1:24,000 pre-eruption orthophotoquads. The extent of pre-eruption clearcut regrowth was obtained from the Forest Management Data Base. Vegetation cover estimates for non-clearcut areas were based on interpretation of color IR photography obtained during the TIMS overflight.

TIMS data processing used ELAS software modules to compute ERT and to georeference the scanner data to the Universal Transverse Mercator (UTM) grid system. Once gridded, sensor and photographic data are registered to topographic maps of the test sites. The LOWTRAN-6 program (developed by the U.S. Air Force Geophysics Laboratory) was run on TIMS data to determine the effects of atmospheric attenuation and meteorological factors on areas scanned by the sensor.

ANALYTICAL PROCEDURES

Forty-three sample plots were selected and gridded in the Tephra Deposition Zone (Test Site A). Average plot size was 30.2 acres. To reduce the effect of slope aspect in measuring effective radiant energy levels, only plots with southeast, south, and southwest facing slopes were used in the study. USDA Forest Service personnel estimated the mean percent vegetation cover for each plot, which ranged from 20 to 100 percent. Using TIMS Band 6 data (11.2-12.2 microns), the mean digital value count was calculated and converted to ERT values. The coefficient of determination (r^2) was calculated for pair values of ERT and percent vegetation cover. The results (r^2 = .9321, Y = .16 x + 19.6, sig. at 0.05 level) show a strong linear relationship between surface ERT and percent vegetation cover.

In the Tree Blowdown Zone, thirty sample plots were selected and gridded. Average plot size was 10.6 acres and post-eruption vegetation cover ranged from 30 to 90 percent. One third of the plots were clearcut prior to the initial eruption; the remaining plots were alpine meadows with less than 70 percent tree cover. Similar to Test Site A, in the Tree Blowdown Zone, ERT and percent vegetation cover showed a relatively strong linear relationship (r^2 = .8276, Y = .12 x + 19.1, sig. at the 0.05 level).

CONCLUSIONS

A method has been described for using the TIMS sensor to monitor vegetation regrowth in primary and secondary disturbance zones on Mount St. Helens. The results of this study demonstrate that the sensor is highly sensitive to vegetation changes. Potentially, TIMS data could be useful in monitoring vegetation patterns over large areas, providing topographic data (e.g., aspect and gradient) are available to be registered with the sensor data.

REFERENCES

Adams, V. D. and Adams, A. B. 1982, Initial Recovery of the Vegetation on Mount St. Helens: in Mount St. Helens One Year Later, edited by S.A.C. Keller: Eastern Washington University Press, Cheney, Washington, 105-114.

Means, J. E. (et al.) 1982, Natural Revegetation of the Northeastern Portion of the Devastated Area: in Mount St. Helens One Year Later, edited by S.A.C. Keller: Eastern Washington University Press, Cheney, Washington, 93-104.

Investigation of Forest Canopy Temperatures Recorded by the Thermal Infrared Multispectral Scanner at H.J. Andrews Experimental Forest

Steven A. Sader

NASA - Earth Resources Laboratory
National Space Technology Laboratories

Thermal Infrared Multispectral Scanner (TIMS) data were collected over the H.J. Andrews Experimental Forest in Western Oregon on July 29, 1983 at approximately 1:30 p.m., Pacific Standard time. Canopy temperatures recorded by TIMS were nearly equal to maximum daily air temperature recorded at eight reference stations. The objective of the investigation was to relate changes in canopy temperature to green leaf biomass levels in reforested clearcuts and old-growth forest. A digital data base was generated in order to isolate that portion of the thermal emission that could be attributed to surface properties (i.e., sun angle effects) other than the vegetation biomass component.

An analysis of variance were performed on the 10 meter data using a randomized complete block design. The null hypothesis was tested: no temperature differences occur between age classes, aspects, or slope gradients. Age classes were used as blocks and the F test revealed that age class and aspect were highly significant but slope and aspect-slope interaction was nonsignificant. Response curves of aspect plotted by slope class for each age class indicated that age class 1 (0-12 years) and age class 2 (13-25 years) were contributing most of the variability in ERT related to terrain positions. The terrain had little effect on ERT for age class 3 (25-33 years) and age class 4 (old growth). The effect of aspect within age class 1 and 2 were tested using single degrees of freedom for each aspect sum of squares. In age class 1, the north aspect had significantly different mean ERT (@ .01 level) from the east,

south, and west aspects. The south aspect in age class 2 was highly significant and north, east and west aspects were nonsignificant.

ERT differences corresponding to aspect and slope variation in age class 1 and 2 may be attributable to the amount of green leaf area and canopy closure present in the sensor field of view. Differential heating and cooling related to sun angle had a greater influence on ERT recorded by TIMS when forest canopies were not completely closed. As the forest matures and the canopy closure and green leaf area approaches maximum, the influence of surface emittance below the canopy contributes less to the total return. This may explain why aspect and slope variation appeared to have little effect on ERT in the older age classes. Near maximum canopy leaf area at H.J. Andrews may occur at around 25 to 30 years on sites replanted to Douglas-Fir.

The TIMS appears to be capable of detecting subtle differences in ERT as related to canopy closure and green leaf biomass, however calibration techniques are needed to correct for emissivity and atmospheric effects. Calibration techniques are the subject of other investigations at the Earth Resources Laboratory in Mississippi. The capability to record surface temperature remotely may become a valuable research tool for forest climatology and hydrology studies where estimates of evapotranspiration rates, plant-water stress and nighttime energy budgets are difficult to measure accurately for large land areas.

Applications of TIMS Data in Agricultural Areas and Related Atmospheric Considerations

R. E. Pelletier and M. C. Ochoa
NASA/NSTL/Earth Resources Laboratory
and Auburn University/Agronomy Department

While much of traditional remote sensing in agricultural research has been limited to the visible and reflective IR, advances in thermal infrared remote sensing technology are adding a new dimension to digital image analysis of agricultural areas. The Thermal Infrared Multispectral Scanner (TIMS) an airborne sensor having six bands over the nominal 8.2-12.2 m range, offers the ability to calculate land surface emissivities unlike most previous singular broad-band sensors. Preliminary findings on the utility of the TIMS for several agricultural applications and related atmospheric considerations are discussed.

Multiple sets of TIMS data were acquired over a highly agricultural region in the Coastal Plain region of Alabama during the spring for maximum bare soil exposure. However, a significant percentage of the fields were in maturing small grain crops, pasture and recently planted corn and peanuts, allowing study of vegetated areas as well. Both predawn and afternoon data sets were obtained to evaluate minimum/maximum thermal diurnal effects. Similarly each pair was collected at three spatial resolutions (5, 10 and 30 m) to evaluate information content based on cell size and atmospheric thickness.

Multiple applications exist for plant studies, soil studies, hydrologic and topographic concerns, inventory and monitoring of conservation practices, and cartographic features extraction. Diseased, water-stressed and maturing crops will demonstrate a greater range in diurnal thermal response than will vigorously growing non-stressed vegetation. Preliminary investigation sug-

gests that relative canopy density can sometimes be determined and that very low density vegetation may be better detected with thermal data than with reflective data. Combinations of these influences may also be useful in identification of different plant types. Determination of certain soil mineralogy is possible due to emissivity variations between bands. Such changes in mineralogy also enables the detection of erosional features. Other soil factors influencing thermal response include porosity and surface condition (e.g. roughness and crustiness). Hydrologic features from small-scale, near-surface soil moisture through larger-scale stream networks, water bodies and related hydrologic features are important components of the thermal imagery. The effects of elevation and aspect can also be seen through differential heating and cooling. Conservation practices such as terraces, grassed waterways and field drainage ditches can be identified often due to moisture differentials. Through data enhancement techniques (e.g. Principal Component Analysis and high-pass filtering) these conservation practices and other linear features such as erosional gullies, field hedgerows, roads, stream networks and water body boundaries can be extracted for cartographic purposes.

Concerns to remove the atmospheric attenuation from TIMS data resulted in a comparison between radiosonde profile data and model atmosphere data from LOWTRAN-6. Comparison of atmospherically corrected graybody (water) spectra to calculated blackbody spectra indicate that small variations in the concentration of water vapor and ozone between the atmospheric models can cause significant distortion in the graybody spectra. TIMS channels 1 and 4 were most altered since the two channels partially overlay water and ozone absorption bands, respectively. Broad geographical seasonal atmospheric models and radiosonde data collected far from the study site should therefore be used with caution.

Locating Subsurface Gravel with Thermal Imagery

Douglas E. Scholen
William H. Clerke
Douglas E. Luepke

U. S. Department of Agriculture
Forest Service
1720 Peachtree Rd.
Atlanta, GA 30367

This paper discusses a method for using 6 band thermal imagery to locate subsurface gravel deposits in vegetated areas. Geologic history is reviewed to select potential areas of study. An overflight is made using a thermal scanner. The data is processed with a computerized system to delineate areas showing a quartz signature radiated by a gravel deposit.

The method was developed during a search for gravel on National Forest land in Louisiana. Processed data from thermal imagery was compared with known gravel deposits and exploratory drill hole logs. A high correlation was noted for a wide range of deposits, from commercial pits to trace deposits only a foot thick. Overburden at these sites varied from zero to sixty feet, near the maximum annual penetration by the thermal wave. It was concluded that the method can be used to locate buried gravel deposits and that more time and effort are needed to verify the usefulness for developing gravel pits adjacent to proposed construction sites.

TIMS DATA APPLICATIONS IN NEBRASKA

Lloyd Queen and Gene Murray, Conservation and Survey Division, Institute of Agriculture and Natural Resources, University of Nebraska-Lincoln, 68588-0517

A total of 172 flight-line miles of TIMS data have been acquired in the state of Nebraska; and an additional mission is planned for August of this year. Data collected by the scanner have generally been applied to investigations in four general areas: hydrology, geology, soils, and vegetation analysis.

Relatively simple manipulations of these thermal-emittance data have led to excellent classifications of vegetation communities established along topographic gradients in the Nebraska Sandhills. Similar procedures were used to study variations in soil parameters along those same gradients.

Virtually all of the spatial variation exhibited in vegetation and in soils is believed to be caused by proximity to subsurface (soil) moisture. Work is currently being conducted in order to examine more closely the relationship between subsurface moisture, vegetation, soil, and surface thermal properties. This work includes the use of diurnal TIMS overflights and consideration of thermal inertia.

Selected hydrologic applications of TIMS data relate to the flow regimes of several Sandhills lakes. Specifically, a "flow-through" model of a natural lake in the Sandhills has been supported through the use of thermal-infrared imager. Also, location and mapping of springs with the use of this thermal scanner is ongoing.

Proposed geologic applications include mapping of the surficial geology along a portion of the Platte River and the delineation of a segment of the Cambridge Arch, a structural geologic feature in central Nebraska.

Remote sensing research being conducted with TIMS is but one component of a larger remote-sensing based investigation of the State of Nebraska. Other systems being utilized include Landsat MSS, Airborne Thermatic Mapper (ATM), Airborne Imaging Spectrometer (AIS), and the Daedalus AADS1260. This large collection of multispectral data over a single area provides unique opportunities for natural resources investigations.

THE APPLICATION OF REMOTELY SENSED DATA TO PEDOLOGIC AND GEOMORPHIC MAPPING ON ALLUVIAL FAN AND PLAYA SURFACES IN SALINE VALLEY, CALIFORNIA

D. A. Miller, G. W. Petersen, and A. B. Kahle[1]

Arid and semi-arid regions yield excellent opportunities for the study of pedologic and geomorphic processes. The dominance of rock and soil exposure over vegetation not only provides the ground observer with unique observational possibilities but also affords good opportunities for measurement by aircraft and satellite remote sensor devices. Previous studies conducted in the area of pedologic and geomorphic mapping in arid regions with remotely sensed data have utilized information obtained in the visible to near-infrared portion of the spectrum. Recently, however, a thermal infrared multispectral scanner for the middle-infrared region of the spectrum has been developed that may prove useful for pedologic and geomorphic studies in arid regions. The Thermal Infrared Multispectral Scanner (TIMS) is an airborne scanner with six channels in the range 8.2 - 12.2 μm. TIMS is normally flown at an altitude that produces a ground resolution of about 30 meters. This is similar to the resolution being achieved by the Landsat-5 Thematic Mapper (TM). The TM sensor collects data in six channels between 0.45 and 2.36 μm and one thermal channel (10.2 - 12.5 μm, 120 meter resolution). Therefore, TIMS and TM provide a range of information from the visible through the middle-infrared portion of the spectrum. Extensive work by researchers at the Jet Propulsion Laboratory (JPL) has shown significant promise for TIMS and TM data in geologic mapping of arid and semi-arid areas. The emphasis of a current research effort being conducted jointly by Penn State University's Office for Remote Sensing of Earth Resources (ORSER) and JPL is to evaluate the ability of TIMS and TM data to aid in the mapping of soils and geomorphic units on alluvial fan and playa surfaces. The area selected for this research is located in the Saline Valley of eastern California. TIMS and TM data collected in 1984 are being used in conjunction with maps compiled during a Bureau of Land Management (BLM) soil survey to aid in a detailed mapping of alluvial fan and playa surfaces within the valley. The results from this study may yield valuable information concerning the application of thermal data and thermal/visible data combinations to the problem of dating pedologic and geomorphic features in arid regions.

---

[1]Graduate student and Professor, Department of Agronomy, The Pennsylvania State University and Supervisor, Geologic Remote Sensing Group, Jet Propulsion Laboratory.

The Red River Valley Archeological Project

Jack Bennett
Archeological Assessments, Inc.
P. O. Box 1631
Nashville, Arkansas 71852

Lawson Smith
Geotechnical Laboratory
U. S. Army Engineering Waterways Experiment Station
P. O. Box 631
Vicksburg, Mississippi 39180

Mark Laustrup
Department of Geography-Geology
University of Nebraska at Omaha
Omaha, Nebraska 68182

The Red River Valley Archeology Project is a long-term effort involving numerous individuals and institutions engaged in archeological investigations in the Texas and Oklahoma portions of the Red River Valley. To date the focus of the project has been on site location. The project acquires both TIMS, TMS, and color infrared photographs over a significant portion of the project area in an effort to define signatures for archeological sites and to assist in the detailed geomorphological mapping of the flood plain. Preliminary analysis of acquired data indicates that both the TIMS and TMS can make a substantial contribution to landform definition, the identification of cultural resources, and to the clarification of site-landform correlations in this riverine environment.

N87-17129

THE PHYSICAL BASIS FOR SPECTRAL VARIATIONS IN THERMAL INFRARED EMITTANCE OF SILICATES AND APPLICATION TO REMOTE SENSING

Louis S. Walter
Laboratory for Theoretical Physics
Goddard Space Flight Center

The use of infrared spectroscopy for the remote characterization of planetary surfaces has received some attention due to efforts in the investigation of these bodies from space. In the 8 to 14 micron region, a depression in the emittance spectra of rocks (sometimes called reststrahlen) is related to the fundamental stretching vibrations of Si-O bonds and shifts in the location of this feature have been ascribed to variations in rock composition.

In 1952, Launer noted that the reststrahlen band shifted to shorter wavelengths as the Si:O ratio of the minerals he was examining increased and correlated the phenomenon with the change in silicate bonding from isolated tetrahedra through chains to framework structures.

The phenomenon he described can be interpreted as being due to the degree of polymerization of SiO4 tetrahedra in silicate minerals. Framework silicates (e.g., quartz, feldspar) are highly polymerized with oxygen linking adjoining silicon cations. In the case of minerals having isolated tetrahedral structures (e.g., olivine), these bridges are broken by other cations (e.g., Mg, Fe). In crystallographic terms, this results in changes in the Si-O bond length and strength which, in turn, affects the location of the reststrahlen band. In 1969, Brown and Gibbs related bond length and strength to the average cation coordination of oxygen in silicate minerals. The oxygen coordination refers to the number of cations bonded to the oxygen anions. For example, the average oxygen coordination for various minerals is: quartz - 2.0; albite/orthoclase - 2.88; pyroxene - 3.33 and olivine - 4.0. They determined a linear relationship between the average coordination number, CN and Si-O, the mean Si-O bond distance: Si-O = 0.015 CN + 1.579 (units in Angstroms). This is the theoretical framework linking the spectral variations in the reststrahlen band and rock mineralogical composition.

Additional theoretical relationships, however, allow us to explore the significance of the spectral features with respect to silicate rock classification inasmuch as some schemes of classification are based, directly or indirectly, on the degree of polymerization of the silicate minerals. For example, the Differentiation Index of Thornton and Tuttle classifies igneous rocks on the basis of the amount of normative quartz, albite and orthoclase (all framework silicate and highly polymerized) relative to other mineral constituents with lower degrees of polymerization. A similar scheme relating silicate rock classification to chemical composition through the thermodynamic effects of polymerization has also been proposed.

Thus, it should be possible to investigate, quantify and model the relationships of reststrahlen spectral band location through silicate mineralogical composition to rock classification. As the Brown-Gibbs relationship is based on the averaged crystallographic properties of minerals,

it is useful for understanding their average thermal IR spectral response which can then be related to the location of the center of gravity of the emittance peaks. However, since in almost all silicates, not all of the oxygen ions are coordinated in the same way, there is a corresponding variation in the bond length and strength. The frequency distribution of the bond strengths is thus related to the spectral curve for a mineral. (This relationship has been used to gain insight into crystal structures as described in a rather large body of literature). Furthermore, the bond strength distribution, integrated over all the minerals in a rock, can next be related to the spectral curve for the whole sample.

It is planned to test these concepts, first through the use of laboratory-acquired data on the IR spectra and mineralogy of selected mineral and rock samples. As a suitable classification model is developed, it will be tested through overflights of appropriate rock outcrops using TIMS.

N87-17130

INFRARED SPECTROSCOPY FOR GEOLOGIC INTERPRETATION OF TIMS DATA

By

Mary Jane Bartholomew
Jet Propulsion Laboratory
California Institute of Technology*
Pasadena, California 91109

Some spectroscopic techniques yield more information directly applicable to the interpretation of TIMS data than others. Clearly, the most meaningful spectra are those collected in the field under climatic, thermal and sky conditions that approximate those at the time of the overflight. The Portable Field Emission Spectrometer, PFES, was designed by JPL with that purpose in mind. It makes normal spectral radiance measurements of the target from 5 to 14 micrometers, has a spectral resolution of approximately 0.2 micrometer, and has an instantaneous field of view of 2 degrees by 10 degrees. The large field of view of the PFES as compared to that readily obtainable in the laboratory with reflectance or emittance instruments makes it indispensible in spectrally analyzing targets with texture or character that varies on a scale greater than one inch.

A team of 3 to 4 people in addition to a small van load of supporting equipment is required to operate the PFES in the field. The spectrometer optics and data reduction system are mounted on backpack frames and day long spectra and sample collecting trips can be undertaken in rough terrane. A number of sedimentary and igneous rocks, all from the western United States have been analyzed.

PFES data reduction is carried out at JPL on a VAX 750. Typically, a target's absolute spectral radiance is determined, a theoretical black body curve, given by Plank's Law, is fit to the data and some measure of the sample's spectral emissivity is found by ratioing the target's spectral radiance to the spectral radiance of the black body.

Two factors have led to interest in laboratory reflectance measurements of rocks and minerals for the purposes of interpreting TIMS data. The first is the cumbersome nature of the PFES, and the second is the tight experimental control available in the laboratory in terms of some of the environmental factors that influence the spectral emission of earth surface materials. The ability to measure total hemispherical reflectance is particularly desirable because data collected at nadir is directly related to the normal spectral emittance of the target by Kirchoff's Law. Strictly specular or diffuse reflectance measurements are not directly related to normal spectral emittance because the geometry of the measurement influences the shape and intensity of absorption features of samples which show wavelength dependent scattering behavior, for example, quartz, Becker et al., 1985.

Nonetheless, I have found the agreement between the bi-conical diffuse reflectance of weathered surfaces of rocks measured in the laboratory and normal spectral emittance of the same samples determined with PFES data to be resonably good. The positions and shapes but not the absolute

intensities of the absorption features in that they occur in both kinds of spectra agree. The reflectance measurements occasionally reveal absorptions not appearing in and/or lost in the noise of the lower resolution PFES spectra. It is encouraging that bi-conical reflectance attachments provide valuable band shape and position information because integrating spheres required for total hemispherical measurements are custom designed and custom built items while bi-conical devices are commonly commercially available under the name of diffuse reflectance attachments.

The future of infrared spectroscopy for geologic interpretation of TIMS data includes the direct laboratory measurement of the normal spectral radiance of earth surface materials at low temperatures (20 to 30 degrees centigrade). We are currently developing this capability at JPL and almost all of the equipment needed has been bought or built and installed. An initial calibration effort is awaiting software development. The major components of the system include a commercially built Fourier Transform infrared spectrometer (the same one used for reflectance measurements), a custom designed sample accessory which is necessary to shield the sample from background radiation and reference blackbodies.

The reflectance measurements of weathered surfaces of rocks that I have made to date have confirmed previous suspicions about the complexity of the spectra of these kind of samples. In particular, heavily weathered or heavily varnished surfaces of rocks have different spectra than the fresh broken surfaces of the same rocks. These observations reemphasize the need to understand the influences of varnish, surface roughness, mineralogy, and particle size on the spectra of naturally occurring rock and mineral surfaces if we are to fully utilize TIMS data to solve geologic problems.

Reference

Becker, F., Ramanatsizehena, P., and Stoll, M.-P., 1985. Angular variation of the bidirectional reflectance of bare soils in the thermal infrared band. Applied Optics, 24, 365-375.

*The research described in this abstract was carried out by the Jet Propulsion Laboratory, California Institute of Technology, under contract with the National Aeronautics and Space Administration.

CALCULATION OF DAY AND NIGHT EMITTANCE VALUES FOR DEATH VALLEY, CALIFORNIA

Anne B. Kahle

Jet Propulsion Laboratory
California Institute of Technology
Pasadena, CA 91109

In July 1983, the TIMS was flown over Death Valley, California on both a midday and predawn flight within a two-day period. The availability of calibrated digital data permitted the calculation of day and night surface temperature and surface spectral emittance.

Image processing of the data included panorama correction and calibration to radiance using the on-board black bodies and the measured spectral response of each channel (Palluconi and Meeks, 1985). Scene-dependent isolated-point noise due to bit drops, was located by its relatively discontinuous values and replaced by the average of the surrounding data values. Bad lines were repaired using values interpolated from adjacent lines. Coherent noise due to microphonics was not removed in these data as it had been in earlier data sets (Kahle, 1983) because it was not judged to be too severe. Both day and night decorrelation- stretched color composite images were created for this Death Valley data set with bands 1, 3, and 5 displayed in blue, green, and red, respectively. As noted in our earlier papers, with this particular band-color display, quartz-rich rocks appear red, carbonates blue-green, and volcanics and shales blue to purple in these images. Comparison of the day-night pair showed that the hues, corresponding to emittance, are similar in the various rock units, while the most striking differences between images are in the intensity of various units, explainable on the basis of day-night temperature effects.

In order to separate the spectral and temperature information contained in these TIMS data, a method is used that was developed by Kahle et al. (1980). It is assumed that the emittance of the ground at every point is equal to 0.93 in the wavelength region of channel six (11.3-11.6 μm). Then Planck's Law

$$L_\lambda = \epsilon_\lambda W_B(\lambda,T) = \frac{\epsilon_\lambda C_1}{\lambda^5[\exp(C_2/\lambda T) - 1]}$$

where: L_λ = measured radiance
W_B = blackbody radiance
λ = wavelength
T = temperature
C_1 = first radiation constant
C_2 = second radiation constant and
ϵ_λ = emittance,

is solved numerically for ground temperature for each pixel in channel 6. Using these temperature values, Planck's Law is then solved in each of the other channels for emittance ϵ_λ.

Both day and night data sets were processed by the above method. There are significant differences to be seen in the day and night temperature images which, as indicated above, were derived from channel 6. In the day image, shaded or north-facing slopes are cooler (darker) than the sun-facing slopes. This illumination-aspect effect disappears in the night image. The very high Panamint Mountains are cold at night due to radiative cooling. Two other areas exhibit striking day-night temperature differences. Middle Basin, in the bottom of the valley floor, has standing water that keeps the area relatively cool (dark) in the day image and relatively warm (bright) in the night image. Conversely, Furnace Creek Fan is very hot in the day image and very cold in the night image. This fan, composed of very low thermal inertia material, bakes dry and becomes very hot in the daytime. At night, water entering the valley at Furnace Creek apparently makes its way to the surface where significant evaporative cooling takes place. A similar effect, of much more limited extent, can be seen at the bottom of the fans coming out of the Panamint Mountains. The ability to detect this effect could be very useful in hydrologic studies.

The emittance images, which were created for channels 1 through 5 for both the day and night data, are shown in Figure 1 with high emittance areas bright. In addition, channels 1, 3, and 5 of the emittance were displayed in blue, green, and red using the decorrelation stretch, for both the day and night data sets. The similarity of the day and night images demonstrates that the procedure for removing the temperature and displaying only emittance is at least qualitatively correct. The emittance images of channel 5 for both day and night (Figure 1) appear quite noisy. This is an artifact introduced by assuming that all emittance values in channel 6 are equal to a constant. Because the emittance in channel 5 is correlated to that in channel 6, it also is being forced towards a constant value -- leaving small dynamic range in the image.

Spectral differences among rock units are consistent from day to night. In Figure 1 the very darkest (low emittance) units in channel 1 are the Eureka and Stirling Quartzite. This is attributed to the strong quartz bands ascribed to the silicon-oxygen stretching vibration (Hunt and Salisbury, 1974). The relatively low emittance of the quartzite becomes less pronounced with increasing wavelength. Alluvial fans which contain abundant quartzite clasts in an argillacious matrix, such as the prominant Tucki Wash and Trail Canyon Fan, are also quite dark, as are their source areas. Spectrally flat carbonates and their derived fans are bright (relatively high emittance) in all channels. The most noticeable changes with wavelength are in the volcanic units including the small andesite outcrop located in the Tucki Wash. These volcanics have a fairly high relative emittance in channel 1 which decreases with increasing wavelength through channel 4, the location of the reststrahlen band of these silicates. These observations are all predictable from laboratory observations (Lyon, 1965).

TIMS is unique in allowing collection of both spectral emittance and thermal information in digital format with the same airborne scanner. For the first time it has been possible to produce day and night emittance images of the same area, coregistered. These data add to an understanding of the physical basis for the discrimination of differences in surface materials afforded by TIMS.

The research described in this paper was carried out by the Jet Propulsion Laboratory, California Institute of Technology, under contract with the National Aeronautics and Space Administration.

REFERENCES

Hunt, G.R., and Salisbury, J. W., 1974, Mid-infrared spectral behavior of igneous rocks: AFCRL-TR-74-0625.

Kahle, A. B., 1983, The new airborne Thermal Infrared Multispectral Scanner (TIMS): IEEE, Proc. International Geoscience and Remote Sensing Symposium (IGARSS '83) **II**, 7.1-7.6.

Kahle, A.B., Madura, D. P., and Soha, J. M., 1980, Middle infrared multispectral aircraft scanner data: analysis for geological applications: Appl. Optics, **19**, 2279-2290.

Lyon, R.J.P., 1965, Analysis of rocks by spectral infrared emission (8 to 25 microns): Econ. Geol., **60**, 715-736.

Palluconi, F. D., and Meeks, G. R., 1985, Thermal Infrared Multispectral Scanner (TIMS): an investigator's guide to TIMS data: Jet Propulsion Lab. Pub. 85-32.

Fig. 1. Emittance images. Top row is emittance derived from the day flight; channels 1-5 from left to right. Bottom row is the emittance derived from the night data.

C-2

APPLICATION OF THERMAL INFRARED MULTIBAND SCANNER (TIMS) DATA TO MAPPING OF PLUTONIC AND STRATIFIED ROCK ASSEMBLAGES IN ACCRETED TERRAINS OF THE NORTHERN SIERRA, CALIFORNIA

James V. Taranik
David Davis
Marcus Borengasser

Department of Geological Sciences
Mackay School of Mines
University of Nevada-Reno

Summary

TIMS data were acquired over the Donner Pass area in California on September 12, 1985. The higher peaks in the area approach 9,200 feet in elevation, while the canyon of the north fork of the American River is only 3000 feet in elevation. The flight altitude above mean terrain was 34,000 feet and the data were acquired at approximately 1330 local time (1930 IRIG). There is 10 to 30 percent vegetative cover in much of the area, although 100% vegetative cover is present in meadows and where soils have developed over metamorphic rocks and capping volcanics. The vegetation is dominated by conifers, although manzanita and other shrubs are present in areas where soils have developed. TIMS data contain noise patterns which cut across scan lines diagonally.

TIMS data were analyzed using both photointerpretative and digital processing techniques. The Jet Propulsion Laboratory produced color images using a decorrelation constrast stretch technique. Initial work was conducted with the JPL photographic prints, although when the original negative was obtained, the image data was printed at 1:40,000 scale for field use. A VAX 11/780 ESL IDIMS image analysis system was used to analyze specific areas at 512 by 512 image resolution. Karhuen-Loeve transformations were utilized to display variations in radiant spectral emmittance. The images were processed according to the receipe developed by the image processing laboratory at JPL. Bands 1, 3, and 5 were selected for the 512 by 512 area. The eigenvectors were calculated for these bands and used in the transformation. The raw principal component images were contrast enhanced using a linear contrast stretch. The enhanced images were united to form a single image on disk. The eigenvectors of the principal component images were calculated and were used to again transform the images. The new principal component images were color encoded so that the image correlated with topography (the one with the most variance) was assigned the color green. The second principal component was assigned the color red and the third principal component was assigned the color blue. The resultant image closely approximated the images produced by JPL. The second and third components appeared to display variations in radiant spectral emittance related to rock composition. The third principal component image largely displayed noise in the image. Only a small portion of the study area has now been field checked, but preliminary analysis has shown that variations in the red colors on the imagery seem to display variation in the silica content of rock materials throughout the area.

The study area lies east of an extensive Mesozoic fault zone that contains large slices of Paleozoic ultramafic rocks and locally metasedimentary rocks. The accreted Paleozoic and Mesozoic rock assemblages have been intruded by plutonic rocks of the Sierra Nevada batholith and are locally capped by Tertiary and Quaternary volcanic rocks. The oldest known rocks of the region belong to the Shoo Fly Complex and the various granitic bodies that were enplaced during Paleozoic time. Some of the granitic bodies are coeval and related to an overlying volcanic rock sequence that ranges in age from Late Devonian to Permian, Schweickert, et. al., (1984). The overlying volcanic sequence is now thought to be the product of a Paleozoic island arc system that was transported from its place of origin and collided with the western edge of North America, Schweickert, et. al., (1984).

The Shoo Fly Complex has been subdivided by Schweickert, Harwood, Girty and Hanson, (1984), into at least four discrete thrust bound units, or allochthons, that were emplaced prior to Devonian time:

1. The Lang-Halsted Sequence. Consists of phyllite and quartzose sandstone with chert and marble.

2. The Duncan Peak Allochthon. Consists mostly of rhythmic, radiolarian and sponge spicule bearing chert and shale with local quartzose sandstone.

3. The Culbertson Lake Allochthon. Vesicular pillow basalt, basaltic breccia, and massive basalt overlain by rhythmically bedded radiolarian and sponge spicule bearing chert and quartz to arkosic sandstones.

4. The Sierra City Melange. Consists of lenses of sheared serpentinite, gabbro, pillowed and massive basalt, ribbon chert, sandstone and small blocks of dolomite.

These assemblages of allochthonous units were elevated as the arc-continent collision progressed and they were probably beveled by wave attack, thus creating a great unconformity, Schwieckert, et. al., (1984). A Paleozoic pyroclastic sequence overlies the Shoo Fly Complex and consists of 8 km. of marine pyroclastic and epiclastic deposits, Schweickert, et. al., (1984). The Pyroclastic Sequence consists of the following lithologies:

1. Grizzly Sierra Buttes Formation, Taylor Formation and lower part of the Peale Formation. Coarse conglomerate, sandstone and argillite which contain chert, quartzite and limestone. Rhyolitic to dacitic tuff, tuff-breccia, and ash flows with black phosphatic chert. Andesitic tuffs and breccias. These rocks are intruded by coeval hypabyssal intrusions that range in composition from andesitic to silicic.

2. The upper Peale Formation. Chert, slate, breccia and tuffaceous material.

3. Goodhue and Reeve Formations. Basalt, basaltic andesite, andesitic breccia containing red chert, tuff, pillow lava and subaerial flows.

The Mesozoic sequence consists of upper Triassic Limestone, the Sailor Canyon Formation which is composed of stratified tuffaceous siltstone and sandstone with minor interbeds of lapilli tuff, and an unnamed volcanic breccia of andesitic composition. The entire sequence of Paleozoic through Jurassic rocks was intruded by batholiths of Jurassic to Cretaceous age and that ranged in composition from granitic to granodioritic.

Preliminary image interpretation and field analysis has confirmed that TIMS image data displays the chert units and silicic volcanics as bright red. The imagery appears to display zoning in the batholitic and hypabyssal intrusive rocks, although this has not been field checked at this time. Rocks which appear to be more dioritic in composition appear purple on the imagery, while rocks more granitic in composition appear shades of red and pink. Areas that have more than 40% vegetative cover appear green on the imagery.

References

Schwieckert, R. A., et. al., 1984, Tectonic development of the Northern Sierra Terrane; an accreted late Paleozoic island arc and its basement: in Western Geological Excursions, Volume 4, Geological Society of America Field Trips 1984 Annual Meeting, pp 1-65.

Presented at: TIMS User's Workshop, National Space Technology Laboratories, Bay St. Louis, Mississippi, June 18-20, 1985 sponsored by Jet Propulsion Laboratory, 4800 Oak Grove Drive, Pasadena, California 91109.

N87-17133

A GEOLOGIC ATLAS OF TIMS DATA

Elsa Abbott

Jet Propulsion Laboratory
California Institute of Technology
Pasadena, California 91109

In the three years since the first data were taken, it has been well demonstrated that TIMS, properly used, can be a most valuable tool for the geologist. We feel that it would be useful to compile the TIMS data available to us at JPL into a geologic atlas. Several data sets have been extensively studied to establish TIMS as a geologic tool and to explore the optimum enhancement techniques. It was found that a decorrelation stretch of bands 1, 3, and 5 enhance the data to a form that is very useful and this enhancement will be used in the geologic atlas along with an accompanying geologic map and description.

Many data sets are well published and familiar to TIMS users, but there are some sets that, for lack of time and funds, have not been thoroughly studied or published. The following is a short description of these least studied sets of data.

In August 1983, two sets of TIMS data were taken over the Valley of Fire area north of Lake Mead in Arizona. A north-south line covers the North Muddy Mountains, an upended section of primarily Mesozoic sediments, including Aztec sandstone; Chinle and Moenkope shales, sandstones and limestones; and Kaibab limestone. Overlapping this data to the south is an east-west line which includes the Valley of Fire and the block of heavily faulted Paleozoic marine carbonates and shales which make up the Muddy Mountain thrust plate.

There are three TIMS data sets of the Southern California batholith taken July 23, 1983. The granitic rocks of this batholith are known to have a small but systematic variation in silica content from southwest to northeast and these data sets include rocks across the range of variation. The most southwesterly set is just inland from the coastal city of Oceanside on the Santa Ana fault block. The area is heavily vegetated with chaparral, but it is possible to distinguish some rock types on the image. In addition to the granitic rocks, which here range from granodiorite to tonalite, the image includes sandstones, gabbro, and undifferentiated metavolcanics. An adjoining data set to the northeast is processed separately across the fault zone which separates the Santa Ana from the Perris fault block. This image, which is also quite vegetated, includes rocks of the batholith, as well as metasediments and older unrelated granitic rocks. Perhaps the most useful data set over this batholith, because it is the least vegetated, is an image covering part of the Little San Bernardino Mountains and Joshua Tree National Monument. The image includes quartz monzonite (partly leucocratic), granodiorite, a gneiss which is very rich in quartz, diorite, gabbro, tonalite, and a pre-Cambrian mixed igneous-metamorphic unit.

A day-night TIMS data set of Pisgah crater area in California's Mojave Desert was taken in July 1983, and added to a rather large collection of infrared data in this area. The TIMS data did not prove as useful as planned because the nighttime data is nearly useless. The daytime data, however, is excellent. The area includes basalts of the Pisgah and Sunshine flows and the older Miocene basalts of Lava Bed Mountains, as well as other igneous rocks of varying compositions, fanglomerates derived from local sources, and the dry bed of Lavic Lake.

Pico anticline in Southern California is a producing oil field in the Santa Susana Mountains just north of San Fernando Valley. It is an area of folded Tertiary sediments made up of sandstone, conglomerate, shale and clay. However, the TIMS image, which was taken in August 1983, is dominated by the heavy cover of chaparral.

There are three TIMS data sets covering the Goldfield mining district in western Nevada. A daytime set was taken in July 1982 and a day-night (5 AM and 12:30 PM) pair were taken in July 1983. Goldfield is a Tertiary volcanic center, possibly a cauldera, which has been altered hydrothermally and enriched in the precious metals which made it one of the richest mining districts in Nevada. Rocks exposed in the area include Mesozoic granitic rocks and shales overlain by Tertiary volcanics, air-fall and ash-flow tuff, intrusive andesite, dacite, rhyo-dacite, quartz latite and rhyolite capped by basalt and welded tuff.

Death Valley has proved to be an excellent study area for TIMS because of the sparse vegetation and varied lithologies exposed, and several well-studied data sets exist of the valley floor and outcrops and alluvial fans west of the valley. East of the valley floor, however, in the Black and Funeral Mountains, there exist TIMS data which has not been fully investigated. There are two day-night sets taken in July 1983 - one north-south and one east-west, covering parts of these mountain ranges. The more northerly Funeral Mountains are predominantly dolomite, quartzite and shale. The Black Mountains are composed of Tertiary volcanic rocks and playa deposits, rhyolite, pre-Cambrian schists and gneisses and basic intrusive rocks.

The images presented along with the many previously studied and published TIMS images constitute an enormously useful set of information for the geologist in the 8-10 μm range. They only await the geologists time and effort.

*The research described in this abstract was carried out by the Jet Propulsion Laboratory, California Institute of Technology, under contract with the National Aeronautics and Space Administration.

Airborne Thermal Infrared Multispectral Scanner Images over Disseminated Gold Deposits, Osgood Mountains, Humboldt County, Nevada

M. Dennis Krohn
U.S.Geological Survey
Reston, Va. 22092

SUMMARY

The U.S. Geological Survey (U.S.G.S.) acquired airborne Thermal Infrared Multispectral Scanner (TIMS) images over several disseminated gold deposits in northern Nevada in 1983. The aerial surveys were flown to determine whether TIMS data could depict jasperoids (siliceous replacement bodies) associated with the gold deposits. TIMS data were collected over the Pinson and Getchell Mines in the Osgood Mountains, the Carlin, Maggie Creek, Bootstrap and other mines in the Tuscarora Mountains, and the Jerritt Canyon Mine in the Independence Mountains. The Osgood Mountain sites were flown by the National Space Technology Laboratory (N.S.T.L.) on mid-morning of 27 August at an altitude of 9150 m; no cloud cover was present.

The sediment-hosted disseminated gold deposits are a major resource for the production of gold in the United States. Gold is disseminated throughout the host rocks in submicroscopic particles, generally less than 5 micrometers (0.005 mm) in size. The sediment-hosted deposits are thought to be low-temperature replacement-type deposits, in which hydrothermal fluids dissolve carbonate minerals and in their place precipitate quartz and fine-grained gold. Prospecting for the deposits is based on geochemical sampling to detect anomalous concentrations of gold, mercury, arsenic, antimony, tungsten, and thallium. Little or no evidence for alteration is present on the surface in these deposits; hence the deposits are referred to as invisible gold, "no-see-em" gold, or bulk-mineable gold deposits. This lack of obvious surface alteration in the host rocks makes detection of disseminated gold deposits a challenge for remote-sensing technology.

A comparison of five major gold deposits in the western United States (Carlin, Cortez, Getchell, Jerritt Canyon, and Pinson) indicates eight geologic characteristics that may be detectable at the surface by different remote-sensing techniques. These characteristics include: 1) silicification of the host limestones to jasperoids, characterized by the Si-O band near 9.3 micrometers; 2) limestone host rocks, characterized by a relatively flat response between 8 and 12 micrometers, except for a sharp band at 11.5 micrometers; 3) organic matter, which is opaque in the near infrared, but may appear transparent in the thermal infrared; 4) argillic/phyllic alteration characterized by several vibrational features between 8 and 14 micrometers; 5) intrusive rocks, characterized by a shift in the Si-O fundamental toward longer wavelenths with increasing mafic composition; 6) calc-silicate minerals possibly characterized by different structure of the bands near 10.8 micrometers; 7) hot-spring deposits which are not directly related to the disseminated gold deposits but show spectral characteristics at the surface related to hydrothermal alteration at depth; and 8) structural features

interpreted by photo-interpretation, which have an important effect on localizing the mineralization in the disseminated gold deposits.

TIMS data of the Osgood Mountains showed a high degree of correlation for the 6 spectral bands between 8 to 12 micrometers. Correlation coefficients were 0.99. Interband correlation was removed by the following steps: 1) a principal component (PC) rotation, 2) a histogram normalization, 3) low-pass filtering of the lower PC components, and 4) the inverse PC rotation. The effect of the transformation on the histograms was to greatly exaggerate small differences observed in the original and intermediate PC data. In the image data, TIMS channel 2 (8.6-8.9 micrometers) is diplayed as red, channel 3 (9.0-9.4 micrometers) as green, and channel 5 (10.3-11.1 micrometers) as blue.

Silicification is the primary geologic characteristic depicted by TIMS. Six types silica-enriched areas are observed on the TIMS image:

1) Primary deposition - Osgood Mountain Quartzite
2) Diagenesis - Chertification of limestone
3) Quartz-vein emplacement - Metamorphic and structural veins
4) Jasperoid formation - Siliceous replacement of limestones
5) Geomorphic deposition - Quartz-rich alluvial fans and dune sand
6) Cultural artifacts - Mine tailings

Most of these features have distinctive morphologies. The larger features, such as the Osgood Mountain Quartzite and the mine tailings, could be discriminated on the TIMS image. The smaller features, such as the jasperoids and the chertified limestones, could not be adequately discriminated at the 25-m resolution of the flight. Density contrasts among these different forms of silicification may make thermal inertia a useful technique in delineating these silica-enriched units.

The interbedded clastic and carbonate rocks of the Preble Formation, a primary host rock for the disseminated gold deposits in the Osgood Mountains, appear to have silica content intermediate between the quartzites and the purer carbonate rocks. Some units that contain both siliceous shales and chert beds resemble the more siliceous units because of preferential resistance of quartz to weathering. A previously unmapped exposure of Preble Formation in a volcanic area was clearly shown on the TIMS data.

The large intrusive plutons of the Osgood Mountain are readily seen on the TIMS image, but smaller cross-cutting dikes are not resolved. Variations within the image appear to correspond to aplite dikes and quartz veins within the pluton. Calc-silicate alteration adjacent to the intrusive bodies, a former source of tungsten, is also seen in the TIMS image and can be distinguished from the more siliceous alteration associated with the disseminated gold deposits. Two younger basalt flows, mapped as the same unit on the geologic map, can be distinguished on the image. Since X-ray and chemical data of the two flows are similar, differences in surface roughness rather than composition may cause the distinctive colors on the image.

Several linear features are observed on the TIMS data as a combination of geomorphic features and tonal alignments. One linear feature was mapped in the alluvium east of the Getchell Mine. It corresponds to a structure mapped by a recent U.S.G.S. telluric survey that has electrical properties similar to the Getchell fault, the main zone of mineralization at the Getchell mine.

TIMS data seem to be a useful supplement to conventional geochemical exploration for disseminated gold deposits in the western United States. Siliceous outcrops are readily separable n the TIMS image from other types of host rocks. Different forms of silicification are not readily separable, yet, due to limitations of spatial resolution and spectral dynamic range. Features associated with the disseminated gold deposits, such as the large intrusive bodies and fault structures, are also resolvable on TIMS data. Inclusion of high-resolution thermal inertia data would be a useful supplement to the TIMS data.

WORKING GROUP DISCUSSIONS

Four separate working groups held discussions of the major issues confronting the TIMS program, and future directions of thermal infrared remote sensing within NASA. These groups were 1) geology, chaired by James Taranik; 2) vegetation, land use and archeology, chaired by James Anderson; 3) data processing, chaired by Michael Abrams; and 4) future directions of the program, chaired by Kenneth Watson. The issues addressed by these groups and their recommendations are summarized here.

GEOLOGY GROUP

Probably the most useful category of ancillary information to the geology group would be a library of lab spectra in the TIMS spectral region, characterized by silicate mineralogy. The group would also like to see a better understanding of the effects of soil moisture, porosity, roughness, vegetation and rock coatings. Perhaps a workshop dealing with physical properties in the thermal IR which was technical and narrowly focused would be very helpful. Additionally there is a need for a bibliography of work done in the thermal IR. It was pointed out that there does exist such a bibliography, possibly not complete enough, which was put together by Herb Blodgett, Code 620, at Goddard Space Flight Center.

As a means of better understanding the nature of things in the thermal IR, there was a desire to see more multiple overflights for modeling; day-night, different altitudes, and at different times of the year for vegetation studies. Some members of the group expressed the desire to have the option of having the image registered to a map, a service which would be useful for areas of very flat terrain. In regard to dealing with the data, there was a call for some means to do atmospheric corrections, either an additional band added to TIMS or another instrument flown in conjunction sensitive to water vapor. The matter of optimal spatial resolution was addressed and it was agreed that it may vary depending upon the use being made of the data. An opinion was expressed that since 30 m resolution is the best we are liable to get from space, perhaps we'd better learn to use it. The need for more experiments to compare data of different resolutions seems called for. The group did not feel they had enough information to recommend any changes in band width or position. The noise level of 0.1 - 0.2 NEΔT was thought to be acceptable.

VEGETATION, LAND-USE AND ARCHAEOLOGY GROUP

The most important need expressed by this group was to have more people in these fields working with TIMS data to define the possibilities of what can be done with it. Basic questions may then be addressed such as the response of vegetation at these wavelengths, if anything species-specific can be learned, and indeed if more can be determined than temperature estimates. The optimal time of day and time of year to take data also needs to be addressed. To attract new users and make the community aware of TIMS, it was suggested that there be a special issue of a remote sensing journal or a special session of a national or international meeting dealing specifically with TIMS. To the same end it was suggested that there be a structured announcement (like an AO or AN) to commit NASA funding and indicate NASA's wish to support TIMS research. A catalog of available data and a

bibliography would offer a start to understanding the usefulness of TIMS as would the availability of a field instrument. To cut the cost of acquiring data the suggestion was made to set up multiple user missions or to piggyback data sets. As far as any desirable changes to the instrument, the group felt they knew of no reasons to do so with the exception that the option to select higher spatial resolution would be helpful.

DATA PROCESSING GROUP

The problems relating to noise in the data was the first topic discussed and the recommendation was made for a document to be sent out with the tape describing all the types of noise known to have been in TIMS data and all that is known about these noise types and their causes. Along with this should be a bibliography of published techniques for noise removal. In addition, it was felt that the filter response curves should be sent, either as a printed document or put on the tape and updated as the calibration is updated. The subject of how to deal with data processing was discussed and it was concluded that a document on how to do data processing was not in order but that a bibliography of sources for data processing would be helpful for the users and perhaps one already exists.

A wish list was compiled by the group which included an independent measurement of temperature, perhaps by adding another channel on TIMS at a wavelength less sensitive to emissivity differences and an independent measure of the atmospheric water, preferrably acquired simultaneously and part of the instrument so there would be no need to co-register the data. Also, costly but desirable new detectors and dewars would help eliminate vibration problems. Additionally, there was a suggestion that we go from the 8-bit to a 10-bit machine since some information is now being lost which could be gained by this move.

FUTURE DIRECTIONS GROUP

Three categories of lab and field studies were identified which are pertinent to understanding what happens in this region of the spectrum; 1) spectroscopic characterization of geologic materials, including alteration or surface coatings and weathering products and processes, 2) spectral emission characteristics of soils as they relate to soil units, and 3) development of surface physical models taking into consideration among other things, surface emissivity, effects of organic materials and water, mixing laws and grain size. Recommendations were made in regard to the aircraft operations which were: 1) to make use of the option of using the C-130 to provide increased range, higher resolution data, and simultaneous acquisition of TIMS, AIS, and TMS data and 2) to keep the TIMS aircraft system intact while putting in a second system if that is to be done so that data acquisition is continuous and interest in the system will not lag. Further possible modifications for the instrument include adding new spectral bands after adequate study of the matter, adding reflective channel(s) to aid in registration, and adding a means to do atmospheric correction. The present signal-to-noise ratio was considered adequate. At the satellite scale it was emphasized that there is a great potential for TIMS-type data on a worldwide basis and support for it needs to begin early, i.e. now for space shuttle or space platform. Bringing together and integrating a team representing diverse disciplines, for example geology, soil sciences and botany, would be strong support for such a satellite program.

SUMMARY

The workshop was a great success, both for the exchange of ideas between investigators and to identify issues of concern to the TIMS program.

One of the major problems identified was that of getting more investigators involved in the program. This need was particularly apparent in the non-geologic disciplines that were represented here - vegetation, land use, and archeology. Suggestions to remedy this included 1) better publicity for the program within the scientific community by way of data catalogues, special issues of journals and symposia, and a published bibliography of infrared research and 2) better support of the TIMS program by NASA including perhaps a structured announcement like an AO or AN to commit NASA funding, and inclusion of the TIMS within the regular structure of the NASA aircraft program, allowing investigators to propose for data flights.

Research issues which were identified as needing more effort and support included 1) spectroscopic characterization of surface materials including rocks, soils, vegetation, surface coatings, and alteration and weathering products, and creation of a data library 2) surface physical modeling to understand effects of surface emissivity, organic materials, porosity, grain size, roughness, and mixing laws 3) studies of parameters for future systems such as spatial and spectral resolution, utility of the 3 - 5 μm window and allowable noise 4) atmospheric corrections using TIMS data and/or ancillary data. The need for a field instrument was emphasized.

With regard to the future of the TIMS program it was recommended that more use be made of the option of operating TIMS on the C-130 to provide increased range, higher resolution and simultaneous TIMS, AIS and NS001 data, along with generally making the data more available to investigators. It was further recommended that if NASA were to opt for an aircraft thermal infrared system with more bands or any other major change, that they do so by building a new scanner while keeping the TIMS aircraft system intact, so that data acquisition is continuous and community interest will not lag. At the satellite scale it was emphasized that there is a great potential for TIMS-type data on a worldwide basis and support for it needs to begin now for space shuttle or space platform.

TIMS WORKSHOP AGENDA

TUESDAY, JUNE 18

Roy Estes	Welcome to NSTL
Anne Kahle	Background of TIMS Program
Chuck Stanich, Thomas Ory	TIMS Instrument
Jerry Meeks	Sensor System Improvements
Frank Palluconi	The TIMS Investigators Guide
James Anderson	Temperature Variations Using TIMS Data
Doug Rickman	The Atmospheric Correction on TIMS Data
Alan Gillespie	Enhancement of TIMS Data For Photo Interpretation
Mel Podwysocki	Use of TIMS Data for Lithologic Mapping in Nevada and Oregon
Phil Christenson	Thermal Imaging Spectroscopy in the Kelso-Baker Region, California
Alan Gillespie	Lithologic Mapping of Silicate Rocks
James Taranik, Amy Hutsinpiller Marcus Borengasser	Detection and Mapping of Volcanic Rock Assemblages and Associated Hydrothermal Alteration with Thermal Infrared Multi-band Scanner (TIMS) Data, Comstock Lode Mining District, Virginia City, Nevada
Ken Watson	Simulation Modeling of TIMS Data and Preliminary Analysis for Carlin and Grapevine, Nevada
Tak Hoshizaki	Preliminary TIMS Data Analysis for Acid Rain Study Sites in Vermont

WEDNESDAY, JUNE 19

Ken Langran	Monitoring Vegetation Recover Patterns of Mount St. Helens
Steven Sader	Thermal Dynamics of H. J. Andrew Experimental Forest
Ramona Pelletier-Travis, Michael Ochoa	The Soils-Agricultural Application for TIMS Data
Doug Scholen, William Clerke Doug Luepke	Locating Subsurface Gravel with Thermal Imagery
Lloyd Queen, Gene Murray	TIMS Data Applications in Nebraska
Doug Miller, Gary Peterson Anne Kahle	The Application of Remotely Sensed Data to Pedologic and Geomorphic Mapping on Alluvial Fan and Playa Surfaces in Saline Valley, California
Jack Bennett, Lawson Smith, Mark Laustrup	Archeology of the Red River Flood Plain
Thomas Sever	Archeological Applications of TIMS Data
Louis Walter	The Physical Basis for Spectral Variations in Thermal Infrared Emittance of Silicates and Application to Remote Sensing
Mary Jane Bartholomew	Infrared Spectroscopy for Geologic Interpretation of TIMS Data
Anne Kahle	Calculation of Day and Night Emittance for Death Valley California
James Taranik, David Davis, Marcus Borengasser	Application of Thermal Infrared Multiband Scanner (TIMS) Data to Mapping of Plutonic and Stratified Rock Assemblages in Accreted Terranes of the Northern Sierra, California
Elsa Abbott	A Geologic Atlas of TIMS Data
Dennis Krohn	Airborne Thermal Infrared Multi-spectral Scanner Images Over Disseminated Gold Deposits, Osgood Mts., Humboldt County, Nevada

THURSDAY, JUNE 20

Discussion Groups

- Geology/Soils
- Botany/Land Use/Archeology
- Data Processing/Noise Removal
- Future Directions

Group Summaries and Conclusions

WORKSHOP PARTICIPANTS

ELSA ABBOTT
MS 183-501
Jet Propulsion Laboratory
California Institute of Technology
4800 Oak Grove Drive
Pasadena, California 91109

MIKE ABRAMS
MS 183-501
Jet Propulsion Laboratory
California Institute of Technology
4800 Oak Grove Drive
Pasadena, California 91109

JAMES ANDERSON
Building 1100
National Space Technology Laboratories
NSTL, Mississippi 39529

MARY JANE BARTHOLOMEW
MS 183-501
Jet Propulsion Laboratory
California Institute of Technology
4800 Oak Grove Drive
Pasadena, California 91109

JACK BENNETT
Archeological Assessments, Inc.
P. O. Box 1631
Nashville, Arkansas 71852

MARCUS BORENGASSER
Department of Geological Sciences
Mackay School of Mines
University of Nevada at Reno
Reno, Nevada 89557

KEN CASHION
Building 1100
National Space Technology Laboratories
NSTL, Mississippi 39529

PHIL CHRISTENSON
Department of Geology
Arizona State University
Tempe, Arizona 85281

BILL CLERKE
U.S. Department of Agriculture
Forest Service
1720 Peachtree Road
Atlanta, Georgia 30367

ROY ESTES
Building 2425
National Space Technology Laboratories
NSTL, Mississippi 39529

ALAN GILLESPIE
MS 183-501
Jet Propulsion Laboratory
California Institute of Technology
4800 Oak Grove Drive
Pasadena, California 91109
on assignment at:
Department of Geologic Sciences
AJ-20
University of Washington
Seattle, Washington 98195

TAK HOSHIZAKI
MS 125-112
Jet Propulsion Laboratory
California Institute of Technology
4800 Oak Grove Drive
Pasadena, California 91109

SUZANNE HUMMER-MILLER
MS 964
U.S. Geological Survey
Denver Federal Center
P. O. Box 25046
Denver, Colorado 80225

ANNE KAHLE
MS 183-501
Jet Propulsion Laboratory
California Institute of Technology
4800 Oak Grove Drive
Pasadena, California 91109

WILLIAM S. KOWALIK
Chevron Oil Field Research
P. O. Box 446
La Habra, California 90631

DENNIS KROHN
MS 927
U.S. Geological Survey
Reston, Virginia 22092

HAROLD LANG
MS 183-501
Jet Propulsion Laboratory
California Institute of Technology
4800 Oak Grove Drive
Pasadena, California 91109

KEN LANGRAN
Building 1100
National Space Technology Laboratories
NSTL, Mississippi 39529

MARK LAUSTRUP
Department of Geography-Geology
University of Nebraska at Omaha
Omaha, Nebraska 68128

JEFF LUVALL
National Space Technology Laboratories
NSTL, Mississippi 39529

JERRY MEEKS
Building 1100
National Space Technology Laboratories
NSTL, Mississippi 39529

DOUG MILLER
Astronomy Department
Tyson Building, 119 Tyson
Penn State University
University Park, Pennsylvania 16802

BOB MURPHY
NASA Headquarters
Code EE
Washington, D.C. 20546

GENE MURRAY
Conservation and Survey Division
Institute of Agriculture and Natural Resources
University of Nebraska at Lincoln
Lincoln, Nebraska 68588-0517

BRAD MUSICK
Building 1100
National Space Technology Laboratories
NSTL, Mississippi 39529

MICHAEL OCHOA
Agronomy Department
Auburn University
Auburn, Alabama 36830

FRANK PALLUCONI
MS 183-501
Jet Propulsion Laboratory
California Institute of Technology
4800 Oak Grove Drive
Pasadena, California 91109

DAVID PARKER
Department of Civil Engineering
Engineering Building 225D
Fayetteville, Arkansas 72701

SANDRA PARKER
Arkansas Archeological Society
P. O. Box 1249
Fayetteville, Arkansas 72702

RAMONA PELLETIER-TRAVIS
Building 1100
National Space Technology Laboratories
NSTL, Mississippi 39529

MEL PODWYSOCKI
MS 927
U.S. Geological Survey
Reston, Virginia 22092

LLOYD QUEEN
Conservation and Survey Division
Institute of Agriculture and Natural Resources
University of Nebraska at Lincoln
Lincoln, Nebraska 68588-0517

DOUG RICKMAN
Building 1100
National Space Technology Laboratories
NSTL, Mississippi 39529

STEVEN SADER
National Space Technology Laboratories
NSTL, Mississippi 39529

DOUG SCHOLEN
U.S. Department of Agriculture
Forest Service
1720 Peachtree Road
Atlanta, Georgia 30367

THOMAS SEVER
Building 1100
National Space Technology Laboratories
NSTL, Mississippi 39529

LAWSON SMITH
Geotechnical Laboratory
U.S. Army Engineering Waterways Experiment Station
P. O. Box 631
Vicksburg, Mississippi 39180

CHUCK STANICH
Daedalus Enterprises
P. O. Box 1869
Ann Arbor, Michigan 48106

JAMES TARANIK
Mackay School of Mines
University of Nevada at Reno
Reno, Nevada 89557

LOU WALTER
Code 620
Goddard Space Flight Center
Greenbelt, Maryland 20771

KEN WATSON
MS 964
U.S. Geological Survey
Denver Federal Center
P. O. Box 25046
Denver, Colorado 80225